Contract No:

This document was prepared in conjunction with work accomplished under Contract No. DE-AC09-08SR22470 with the U.S. Department of Energy (DOE) Office of Environmental Management (EM).

Disclaimer:

This work was prepared under an agreement with and funded by the U.S. Government. Neither the U. S. Government or its employees, nor any of its contractors, subcontractors or their employees, makes any express or implied:

1) warranty or assumes any legal liability for the accuracy, completeness, or for the use or results of such use of any information, product, or process disclosed; or
2) representation that such use or results of such use would not infringe privately owned rights; or
3) endorsement or recommendation of any specifically identified commercial product, process, or service.

Any views and opinions of authors expressed in this work do not necessarily state or reflect those of the United States Government, or its contractors, or subcontractors.

October 4, 2017

SRNS-E1122-2017-00009
RSM Track #:10667

TO: M. G. SERRATO, 773-42A

FROM: J. M. CARTER, 704-2H

US ARMY CORPS OF ENGINEERS – ENGINEERING RESEARCH AND DEVELOPMENT CENTER – PETROGRAPHIC ANALYSIS OF SECTION 3 PERSONNEL TUNNEL CONCRETE

References:
1. C-ESR-H-00044, Rev. 0, H-Area Canyon Exhaust (CAEX) Tunnel Concrete Core Sampling Plan
2. C-DCP-H-16006, Rev. 0, Concrete Coring and Sleeve Assembly Installation in the 221-H Section 3 Personnel Tunnel

Attached is the June 2017 US Army Corps of Engineers – Engineering Research and Development Center (ERDC) evaluation of concrete cores taken from the 221-H Section 3 Personnel Tunnel North and South Walls. The South wall of the Personnel Tunnel is adjacent to soil. The North wall of the Personnel Tunnel is adjacent to the Canyon Exhaust Cross-Over Tunnel, which contains the exhaust air flows from the Canyon and HB-Line processes.

Due to low compressive strength test results from the North wall cores, the U.S. Department of Energy, Savannah River, requested ERDC to evaluate and determine the cause for the low compressive strength. Several concrete cores from the North and South Walls were provided to ERDC. The attachment contains the ERDC evaluation and analysis.

Attachment

cc: S. A. Carey, 730-2B
G. S. Elchoufi, 730-2B
C. A. Langton, 773-42A
A. J. Duncan, 773A

SRNS-E1122-2017-00009

US Army Corps of Engineers®
Engineer Research and Development Center

ERDC
INNOVATIVE SOLUTIONS for a safer, better world

Petrographic Analysis of H-Canyon Section 3 Personnel Tunnel Concrete

Cody M. Strack, Erin R. Reed-Gore, Kyle L. Klaus, and Jason Morson and Robert D. Moser

June 2017

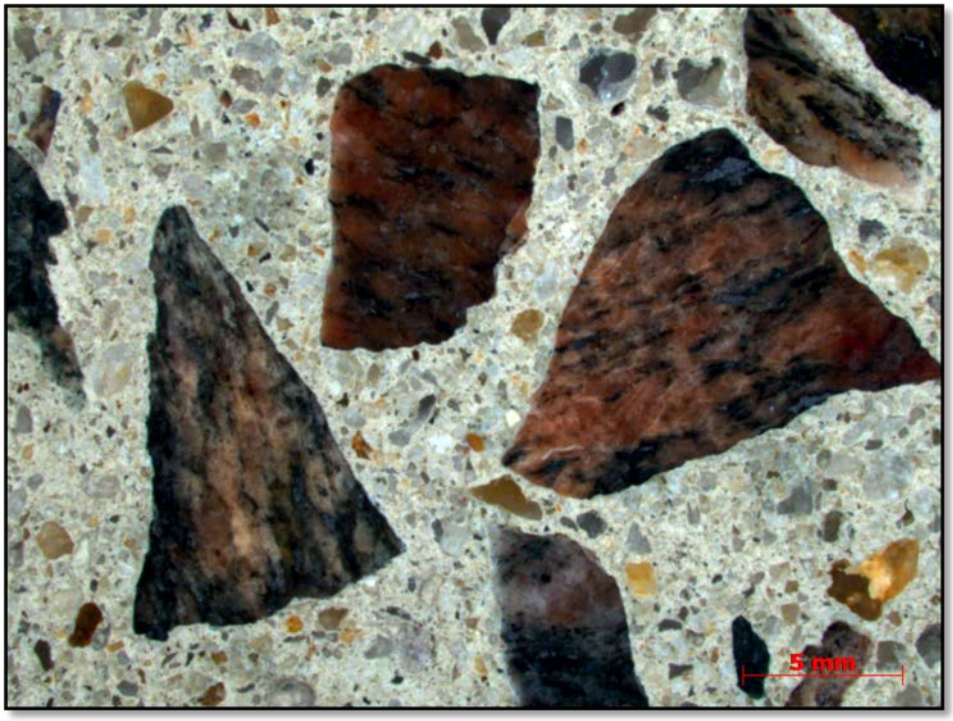

For public release; distribution unlimited.

Engineer Research and Development Center

Executive Summary

The Concrete and Materials Branch (CMB) of the Geotechnical and Structures Laboratory was requested to perform an analysis on concrete cores collected from the north and south walls of the H-Canyon Section 3 Personnel Tunel, Savannah River Site, Aiken, South Carolina to determine the cause of the lower than expected compressive strength. This study examined five cores provided to the ERDC by the Department of Energy. The cores were logged in as CMB No. 170051-1 to 170051-5 and subjected to petrographic examination, air void analysis, chemical sprays, scanning electron microscopy, and x-ray diffraction.

The results of the study indicated the low compressive strength can be attributed to:

- High clay content in the original concrete mix. The clay is concentrated at the fine and coarse aggregate surfaces which has resulted in poor aggregate-paste bonding. It is also present in the paste fraction and therefore contributes to a lower strength matrix.

- High water to cement ratio estimated to be approximately 0.5 in the North Wall concrete and >0.5 in the South Wall concrete. This is estimated from capillary porosity and shrinkage cracking per scanning electron microscopy analyses.

- Higher volume of entrained/entrapped air.

From the observations in this study, there does not appear to be an active, deleterious process such as ASR that caused or will continue to cause a loss in strength in either wall. Mineralogical analysis of the cement fraction for four samples were mainly comprised of tobermorite, an alteration product of portland cement. Results of air void analysis of the 2 samples from the south wall yielded similar results, while samples from the north wall had variations in percent air content. Calculated mixture proportions for all the samples were roughly the same.

Overall, the low compressive strength observed in the north wall compared with the south is attributable to the increased abundance of clay coatings on aggregates, higher observed capillary porosity, and increased air content.

Contents

Figures and Tables

Figures

Tables

Preface

This study was conducted in support of the U.S. Department of Energy Savannah River Site. The technical monitor was Dr Robert D. Moser of the U.S. Army Engineer Research and Development (ERDC).

The work was performed by the Concrete and Materials Branch (GMC), of the Engineering Systems and Materials Division (GM), US Army Engineer Research and Development Center (ERDC), Geotechnical and Structures Laboratory (ERDC-GSL). At the time of publication, Christopher M. Moore was Chief, CEERD-GMC; Dr Gordon W. McMahon was Chief, CEERD-GM. The Deputy Director of ERDC-GSL was Dr William P. Grogan and the Director was Mr. Bart Durst.

COL Bryan Green was the Commander of ERDC, and Dr David W. Pittman was the Director.

1 Scope

The Concrete and Materials Branch (CMB) of the Geotechnical and Structures Laboratory was requested to perform an analysis on a concrete wall samples retained from the north and south walls of the H-Canyon Section 3 Personnel Tunnel. A total of four cores and one over core were provided to the CMB, which were checked in under CMB Serial Number 170051. Two were extracted from the south wall (170051-1, 170051-2) and three from the north wall (170051-3, 170051-4, 170051-5). Table 1 lists the cores received with the original sample identifier, core length, and the lab tests performed for each core. Due to the condition in which core 170051-5 was received, only select tests were performed. The results of this analysis will dictate the path forward for repairs on the structure.

The following sections provide a summary of the methods utilized, results obtained from each core, and a summary of the investigation.

Table 1. Summary of cores received, corresponding CMB Serial No., core length, and lab tests performed.

CMB ID	SNRS Core ID	Core Length	Lab Test Performed
170051-1	221H-PT3-S-2-D	7 in.	ASTM C-856, ASTM C-457, XRD, chemical sprays, optical microscopy, electron microscopy
170051-2	221H-PT3-S-6-D	6 in.	ASTM C-856, ASTM C-457, XRD, optical microscopy, electron microscopy
170051-3	H221-PT3-N-1	7.5 in.	ASTM C-856, ASTM C-457, XRD, optical microscopy, electron microscopy
170051-4	221-H-PT3-N-2-B	6 in.	ASTM C-856, ASTM C-457, XRD, optical microscopy, electron microscopy
170051-5	H-PT3-N-4	Over core was not intact upon receipt	ASTM C-856, ASTM C-457, and optical microscopy

2 Methods

Testing was conducted to determine the mineralogical constituents of the concrete and any possible chemical reactions and microstructural deterioration present. The following describes the methods utilized.

2.1 Petrographic Analysis

Modes of distress such as sulfate attack, microcracking, and overall concrete quality were assessed by visual examination of the as received cores as well as a petrographic analysis performed on polished cross sections conducted according to ASTM C856 - *Standard Practice for Petrographic Examination of Hardened Concrete*. A 25 mm thick section of a core was cut and prepared for the petrographic analysis. The section for petrographic analysis was polished using diamond incrusted polishing pads. The polished sample was imaged using a Zeiss Stereo Discovery V20 microscope at magnifications of 5 X to 40 X. An overall image was obtained for the sample at low magnification, and at least three selected sites were also imaged at higher magnification. Specific focus was given to microcracking, air void structure, aggregate deterioration, and any other possible modes of concrete deterioration that are relevant for service life estimation.

2.2 Scanning Electron Microscopy (SEM)

Specimens were examined from each sample using scanning electron microscopy (SEM) to obtain high-resolution images and examine the paste microstructure according to ASTM C1723 – *Standard Guide for Examination of Hardened Concrete Using Scanning Electron Microscopy*. 15mm diameter cores were taken from each sample, mounted in epoxy, and polished to 0.3µm in a 50:50 ethanol and ethylene glycol mixture prior to imaging. SEM imaging was performed using an FEI Nova NanoSEM 630, capable of high-resolution imaging on non-conductive materials. Imaging was performed in low-vacuum mode at pressures of 0.1-0.5 mbar and accelerating voltage of 15kV. All images were acquired using a backscattered electron detector to improve phase contrast. Imaging was performed at three random sites and at various levels of magnification to capture the overall microstructure along with specific regions of interest (e.g., aggregate interfaces, cracks, air voids).

2.3 X-ray Diffraction Analysis

X-ray diffraction (XRD) analysis was performed to identify the mineralogy of each component present in the concrete according to ASTM C1365 – *Standard Test Method for Determination of the Proportion of Phases in Portland Cement and Portland-Cement Clinker Using X-Ray Powder Diffraction Analysis*. Once the desired sample was isolated from the concrete, it was crushed and ground until at least 90% of the material passed a #325 sieve (44 µm). The ground specimen was prepared into random powder pack sample holders for XRD measurements. Diffraction patterns to be used for qualitative phase identification were obtained using a Panalytical X'Pert Pro materials research diffractometer equipped with a Co-Kα X-ray source operated at 45kV and 40mA. Diffraction patterns were obtained over a period of 2 hr from 2 to 70 °2Θ with a step size of 0.02 °2Θ. Phase identification was performed using MDI Jade2010 powder diffraction file (PDF) reference databases.

2.4 Chemical Spray Indicator Testing

Alkali-Silica Reaction

The presence of ASR was determined by the use of ASR-specific chemical stains, Rhodamine B and Sodium Cobaltinitrite. The test was applied to a freshly fractured surface. Surface preparation involved wetting with deionized water, followed by treating with two staining agents. The first stain applied was Sodium Cobaltinitrite, which was left on the surface for approximately 60 sec. The surface was rinsed with deionized water to remove excess stain. The persistence of a yellow color indicates the presence of potassium-rich silica gels, generally thought to represent active ASR. After the second rinse was finished, the second staining agent, Rhodamine B, was applied; and the excess was rinsed off after approximately 60 sec. This stain leaves a pink color in locations containing calcium-rich silica gels that are generally thought to represent older ASR.

Carbonation Depth

Phenolphthalein, pH indicator, was also used to determine the depth of carbonation / acidification of the concrete. This indicator exhibits a bright pink colour when exposed to alkaline concrete and remains clear when concrete is carbonated (pH below ~10). The test was applied to a freshly

fractured surface. Surface preparation involved wetting with deionized water, followed by treating with phenolphthalein.

2.5 Air Void Analysis ASTM-C457 / Phase Fraction Analysis

Air void content was determined according to the provisions outlined in ASTM C457 – *Standard Test Method for Microscopical Determination of Parameters of the Air-Void System in Hardened Concrete*. The air voids characterized included spaces enclosed by cement paste that were filled with air or other gas prior to setting of the paste. Voids measured included both entrapped and entrained air larger than a few micrometers in diameter. The air voids characterized by ASTM C457 do not include lower length scale voids associated with the cement hydration products themselves. As a result, air void content measurements are less than total porosity of the concrete and are an indicator of air void systems that are associated with resistance of the concrete to cyclic freezing and thawing. Along with characterizing the hardened air void structure, additional information was gathered through point counting on the paste, aggregate, and other observed defects. The test method has two procedures; Procedure A, Linear-Traverse Method and Procedure B, Modified Point-Count Method of which was used for this study. Procedure B was employed for the analysis described herein. Samples were cut and polished cross sections prepared according to ASTM C856 - *Standard Practice for Petrographic Examination of Hardened Concrete*. The minimum length of traverse and minimum number of points for the point count method was determined based on the maximum size of aggregated found in each sample. Calculations for air content were determined on the total number of air voids (N), total number of stops (S_t), number of stops in air voids (S_a), number of stops on paste (S_p), and the E-W translation distance between stops (I).

3 Results and Discussion

3.1 Core Sample 170051-1 – 221H-PT3-S-2-D

The core was extracted from the south wall of the personnel tunnel. It was seven inches in length and three and three/fourths inches in diameter (Figure 1). Cracking was not observed on the surface, nor throughout the exterior of the core. The surface of the core had been in contact with a sheet pile panel rib that caused a cylindrical impression (Figure 2).

3.1.1 Petrographic Analysis

Low (5x) and high (10x, 12x) magnification photomicrographs of the typical microstructure observed in concrete specimen 170051-1 are presented in Figure 3. The coarse aggregate is uniformly distributed and appears to make up 40 percent of the volume. The coarse aggregate is interpreted to be a metamorphic siliceous creek rock gravel and ranged from one to two inches in size. They are sub-angular to angular with a small portion being elongate. The fine aggregate made up approximately 40 percent of the volume and was sub-angular to sub-round in shape. It is interpreted to be crushed quartz sand amongst other siliceous minerals. The core showed a discoloration of the paste content from light grey (N7) to moderate orange pink (10R 7/4) that penetrated up to four centimeters (Figure 3). The change is not gradual and marks two distinct zones. The colors and their codes were determined by comparison with the Munsell Rock Color Book. There were few signs of cracking or infilling, thus it is suspected to not have suffered ASR-related deterioration. Internal cracks within the coarse aggregate are rare and are interpreted to represent pre-existing damage.

Figure 1. As received core sample 170051-1.

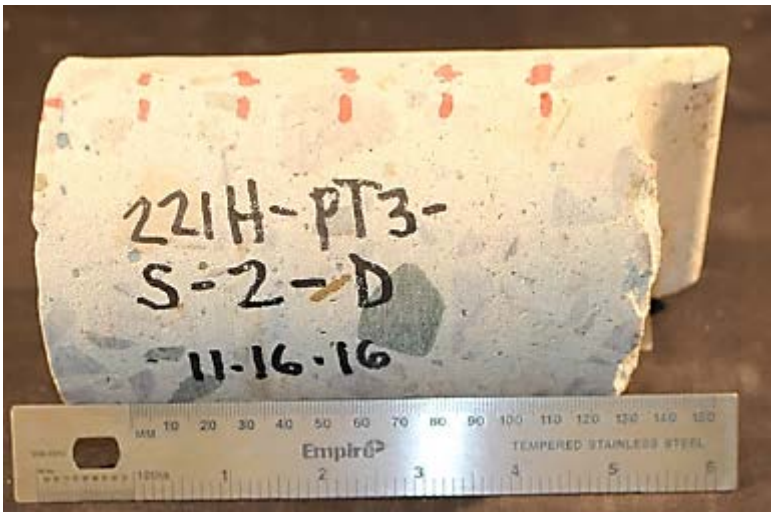

Figure 2. As received core sample 170051-1 showing impression and discoloration of cement where the concrete was in contact sheet pile material.

Figure 3. Low and high magnification photomicrographs of 170051-1 (a) Surface edge of core with coarse aggregate and moderate orange pink colored paste (b) Coarse aggregate (c) High magnification of the core exhibiting the color change of the paste fraction of the concrete in addition to a concentration of air voids (d) Coarse aggregate with preexisting fractures.

(a) 5x magnification photomicrograph

(b) 5x magnification photomicrograph

(c) 10x magnification photomicrograph

(d) 5x magnification photomicrograph

3.2 Core Sample 170051-2 – 221H-PT3-S-6-D

The core was received from the south wall of the personnel tunnel. It was 6 inches in length and three and three/fourth inches in diameter (Figures 4 and 5). Cracking was not observed on the surface, nor throughout the body of the core.

3.2.1 Petrographic Analysis

Low and high magnification photomicrographs of the typical microstructure observed in concrete specimen 170051-2 are presented in Figure 6. The coarse aggregate is uniformly distributed and appears to make up 40

percent of the volume. The coarse aggregate is interpreted to be a metamorphic siliceous creek rock gravel and ranges from one to two inches in size. They are sub-angular to angular with a small portion being elongate. The fine aggregate made up approximately 40 percent of the volume and was sub-angular to sub-rounded in shape. It is interpreted to be crushed quartz sand amongst other siliceous minerals. The paste content was light grey (N7). This color and its code were determined by implementing the Munsell Rock Color Book. There were few signs of cracking or infilling, thus it is suspected to not have suffered ASR-related deterioration. Internal cracks within the coarse aggregate are rare and are interpreted to represent pre-existing damage.

Figure 4. As received core sample 170051-2.

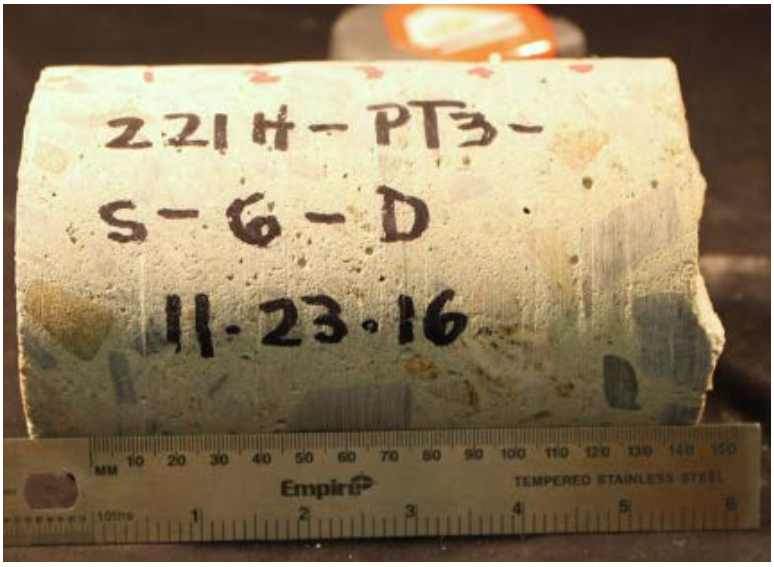

Figure 5. As received core sample 170051-2.

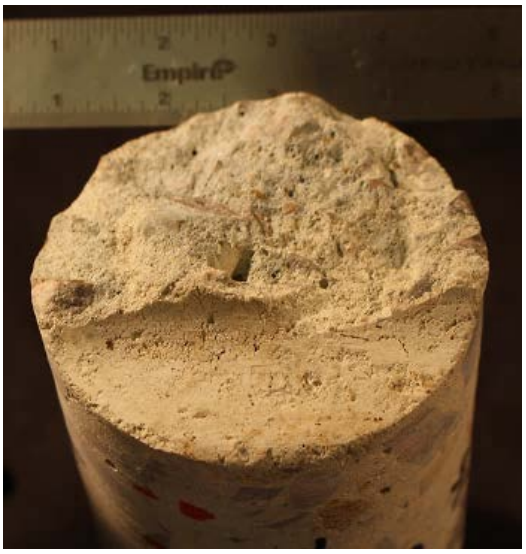

Figure 6. Low and high magnification photomicrographs of 170051-2 (a) Surface edge of core with coarse aggregate (b) Coarse aggregate (c) High magnification of the core showing large void near aggregate (d) High magnification of fine aggregate and paste

(a) 5x magnification photomicrograph

(b) 5x magnification photomicrograph

(c) 10x magnification photomicrograph

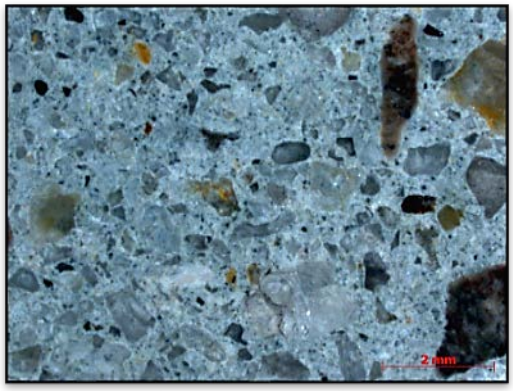

(d) 12x magnification photomicrograph

3.3 Core Sample 170051-3 – H221-PT3-N-1-B

The core was received from the north wall of the personnel tunnel. It was seven and a half inches in length and three and three/fourth inches in diameter (Figure 7). Cracking was not observed on the surface, nor throughout the body of the core.

3.3.1 Petrographic Analysis

Low and high magnification photomicrographs of the typical microstructure observed in concrete specimen 170051-3 are presented in Figure 8. The coarse aggregate is uniformly distributed and appears to make up 40 percent of the volume. The coarse aggregate is interpreted to be a metamorphic siliceous creek rock gravel and ranges from one to two inches in size. They are sub-angular to angular with a small portion being elongate. The fine aggregate made up approximately 40 percent of the volume and was sub-angular to sub-rounded in shape. It is interpreted to be crushed quartz sand amongst other siliceous minerals. The paste content was pale yellowish brown (10YR 6/2). This color and its code were determined by implementing the Munsell Rock Color Book. There were few signs of cracking or infilling, thus it is suspected to not have suffered ASR-related deterioration. Internal cracks within the coarse aggregate are rare and are interpreted to represent pre-existing damage.

Figure 7. As received core sample 170051-3

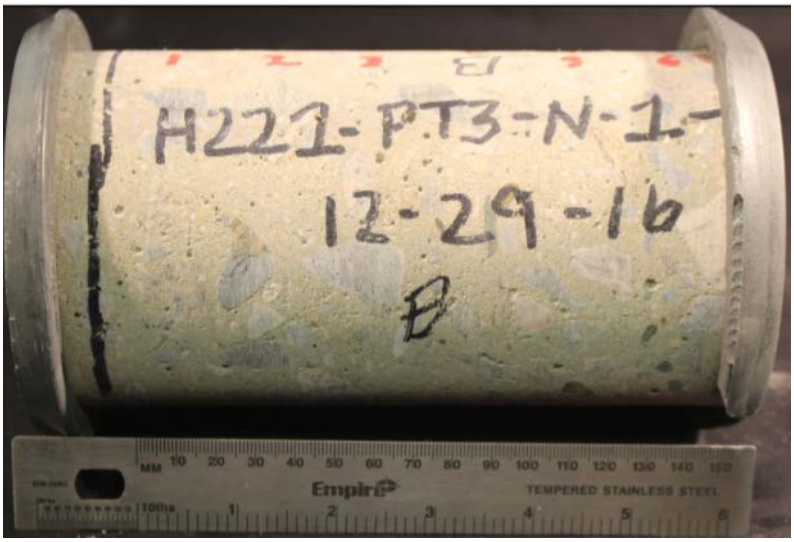

Figure 8. Low and high magnification photomicrographs of 170051-3 (a) Edge of core with coarse aggregate (b) Large coarse aggregate (c) High magnification of the core showing coarse aggregate (d) High magnification of fine aggregate and air void

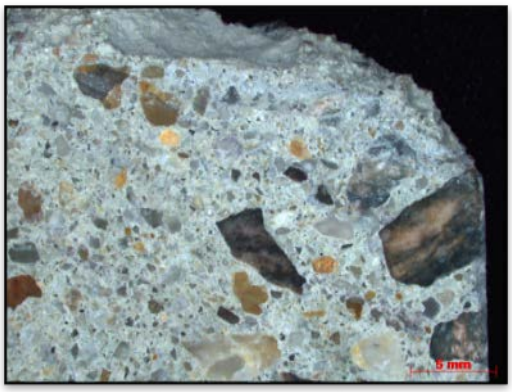

(a) 5x magnification photomicrograph

(b) 5x magnification photomicrograph

(c) 5x magnification photomicrograph

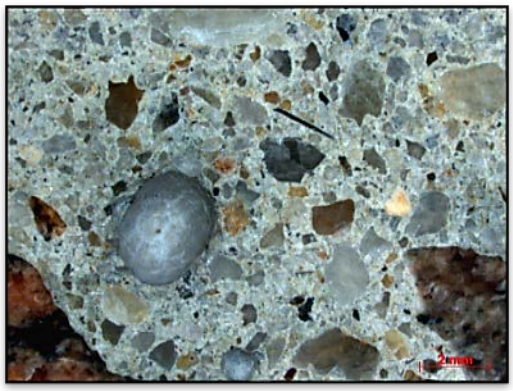

(d) 10x magnification photomicrograph

3.4 Core Sample 170051-4 – 221-H-PT3-N-2-B

The core was received from the north wall of the personnel tunnel. It was six inches in length and three and three/fourth inches in diameter (Figure 9). Cracking was not observed on the surface, nor throughout the body of the core.

3.4.1 Petrographic Analysis

Low and high magnification photomicrographs of the typical microstructure observed in concrete specimen 170051-4 are presented in Figure 10. The coarse aggregate is uniformly distributed and appears to make up 40 percent of the volume. The coarse aggregate is interpreted to be a metamorphic siliceous creek rock gravel and ranges from one to two inches in size. They are sub-angular to angular with a small portion being elongate.

The fine aggregate made up approximately 40 percent of the volume and was sub-angular to sub-rounded in shape. It is interpreted to be crushed quartz sand amongst other siliceous minerals. The paste content was pale yellowish brown (10YR 6/2). This color and its code were determined by implementing the Munsell Rock Color Book. There were few signs of cracking or infilling, thus it is suspected to not have suffered ASR-related deterioration. Internal cracks within the coarse aggregate are rare and are interpreted to represent pre-existing damage.

Figure 9. As received core sample 170051-4

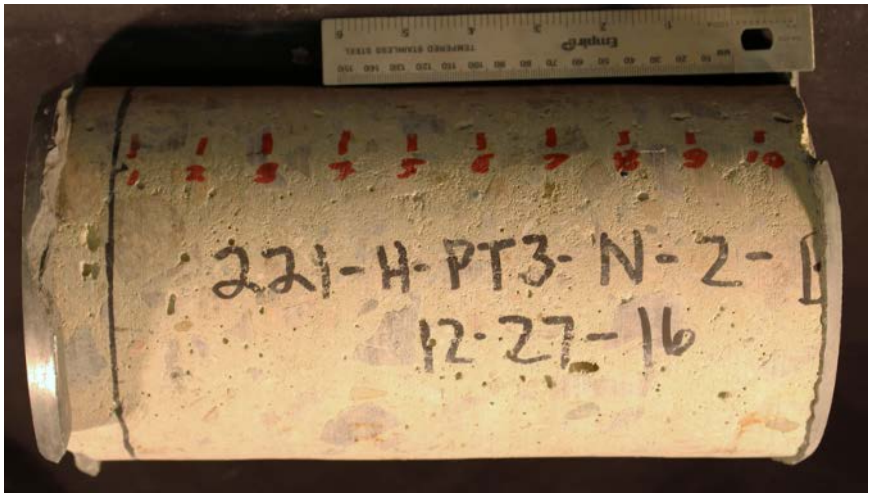

Figure 10. Low and high magnification photomicrographs of 170051-4 (a) Edge of core with coarse aggregate (b) Large impression of debonded coarse aggregate in which a high volume of air voids are observed (c) High magnification large air void (d) High magnification of fine aggregate and paste

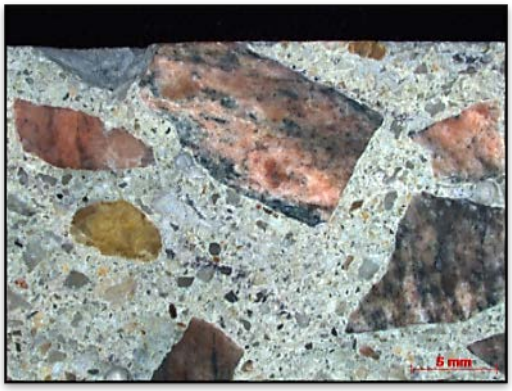

(a) 5x magnification photomicrograph

(b) 5x magnification photomicrograph

(c) 10x magnification photomicrograph

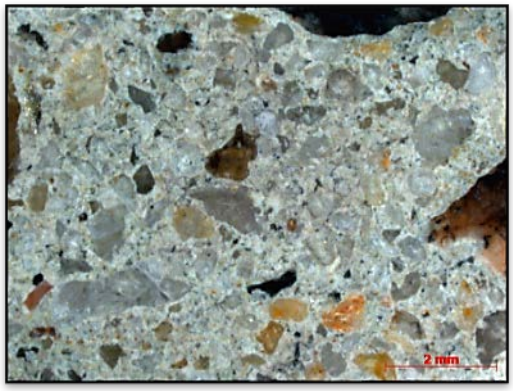

(d) 12x magnification photomicrograph

3.5 Core Sample 170051-5 – H-PT3-N-4

The as received over-core was from the north wall of the personnel tunnel. The sample broke during shipping and was not intact (Figure 11). As such, distinguishing between original and transport-related damage was difficult.

3.5.1 Petrographic Analysis

Low and high magnification photomicrographs of the typical microstructure observed in concrete specimen 170051-5 are presented in Figure 12. The coarse aggregate is uniformly distributed and appears to make up 40 percent of the volume. The coarse aggregate is interpreted to be a metamorphic siliceous creek rock gravel and ranges from one to two inches in

size. They are sub-angular to angular with a small portion being elongate. The fine aggregate made up approximately 40 percent of the volume and was sub-angular to sub-rounded in shape. It is interpreted to be crushed quartz sand amongst other siliceous minerals. The paste content was pale yellowish brown (10YR 6/2). This color and its code were determined by implementing the Munsell Rock Color Book. Due to the state in which the core was received, making conclusions based off cracks seen within the core is not advised. Internal cracks within the coarse aggregate are rare and are interpreted to represent pre-existing damage.

Figure 11. As received core sample 170051-5

Figure 12. Low and high magnification photomicrographs of 170051-4 (a) Edge of core with coarse and fine aggregate (b) Coarse aggregate (c) High magnification of a crack following the edge of a coarse aggregate (d) High magnification of fine aggregate and paste.

(a) 5x magnification photomicrograph

(b) 5x magnification photomicrograph

(c) 12x magnification photomicrograph

(d) 12x magnification photomicrograph

3.6 Scanning Electron Microscopy (SEM)

A 200x magnification montage image of the paste and fine aggregate microstructure for 170051-1 is shown in Figure 13 with phases indicated. Clays are primarily seen at the particle-paste boundary. High magnification images (Figure 14, 15) feature unhydrated cement particles, capillary pores, and some microcracking. The presence of secondary cementitious materials was not observed. Considerable capillary pore space suggests a water cement ratio of at least 0.50. In some cases, the capillary pores connect, creating networks of void space.

Figure 13. 200x magnification SEM montage of microstructure for 170051-1.

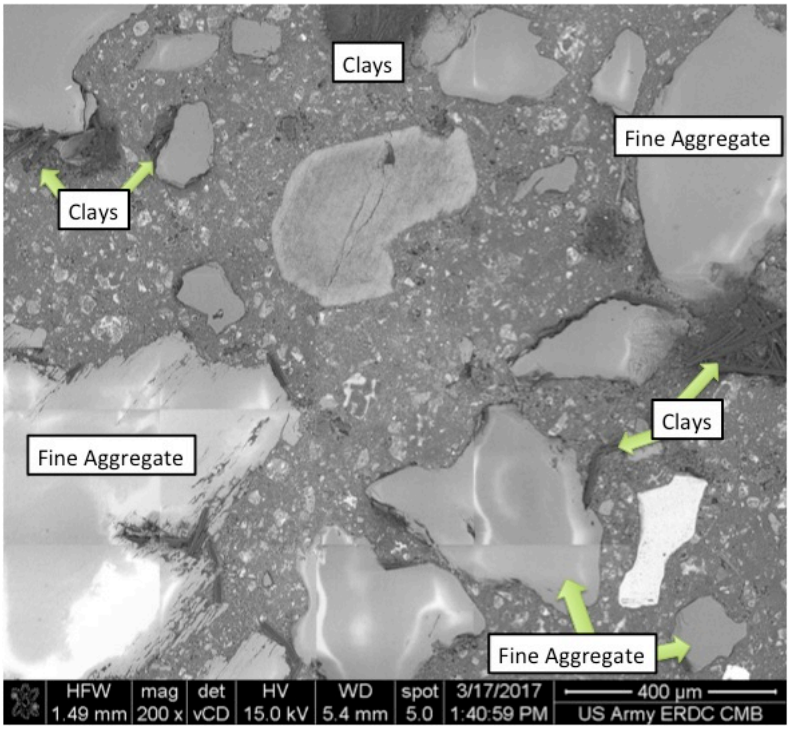

Figure 14. 1000x magnification SEM image of paste microstructure for 170051-1. The image shows regions of high capillary porosity, microcracking with a portion infilled, and unhydrated cement

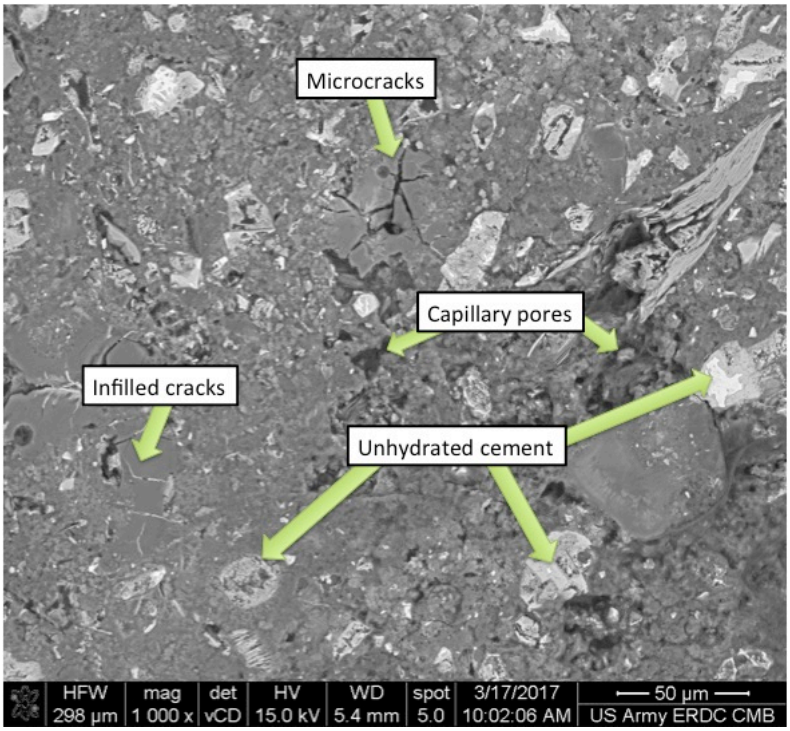

Figure 15. 1000x magnification image of paste microstructure for 170051-1 illustrating unhydrated cement grains, high capillary porosity, and microcracks.

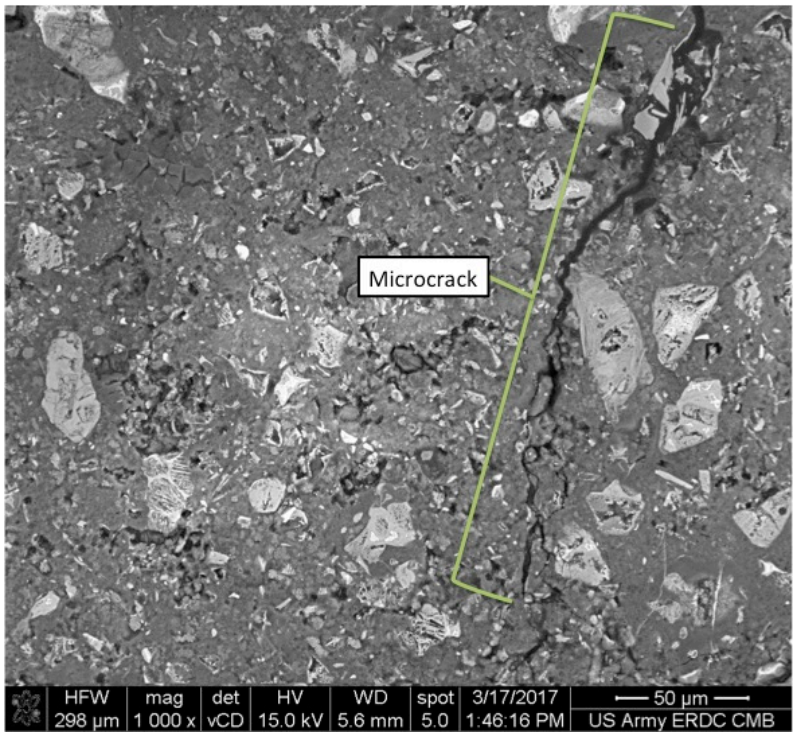

A low magnification montage image of the concrete microstructure for 170051-2 is shown in Figure 16 with phases indicated. Clays are primarily seen at the particle-paste boundary. High magnification images (Figure 17, 18) feature unhydrated cement particles, capillary pores, and some microcracking. In Figure 17, pores are observed at the paste/aggregate boundary. The presence of secondary cementitious materials was not observed. Capillary pore space suggests a water cement ratio of at least 0.50. At high magnification small cracks are visible.

Figure 16. 220x magnification montage of microstructure for 170051-2 illustrating fine aggregates with occasional clay minerals attached and unhydrated cement particles.

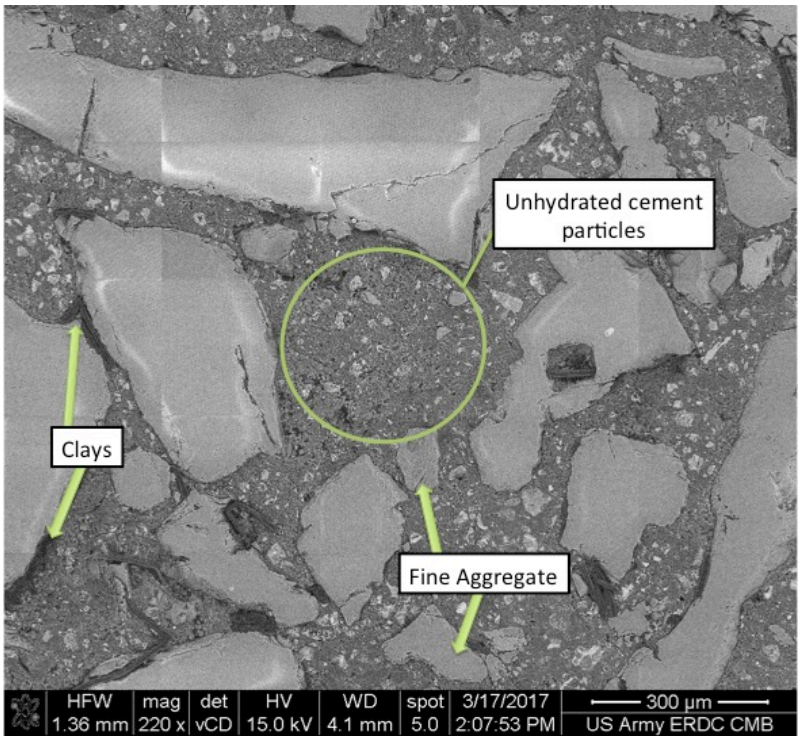

Figure 17. 1000x magnification image of paste microstructure for 170051-2 illustrating regions of high capillary porosity and a large number of unhydrated cement grains.

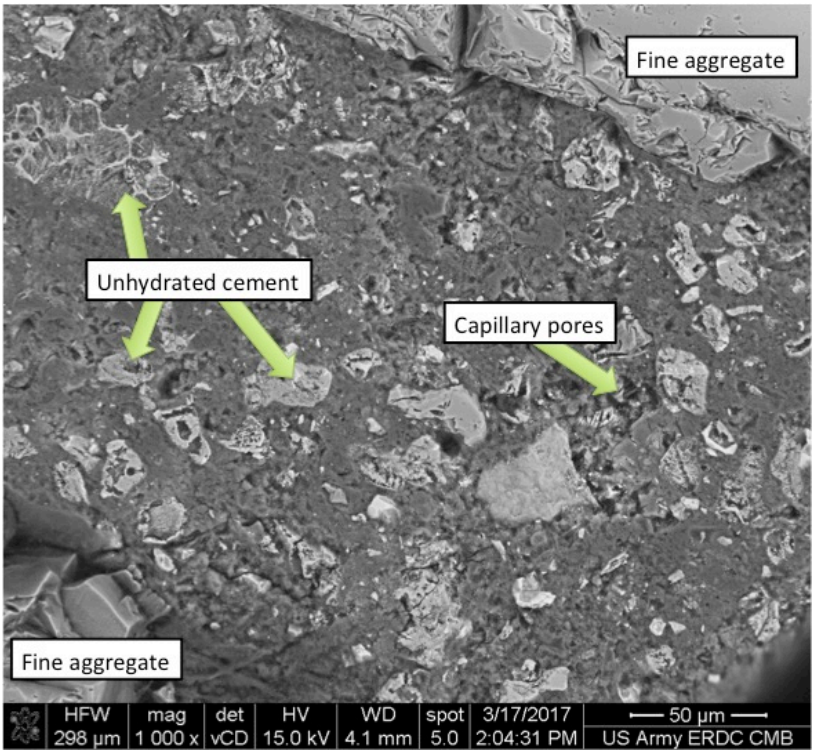

Figure 18. 4000x magnification image of paste microstructure for 170051-2 showing the existence of microcracks, high capillary porosity, and calcium silicate hydrate.

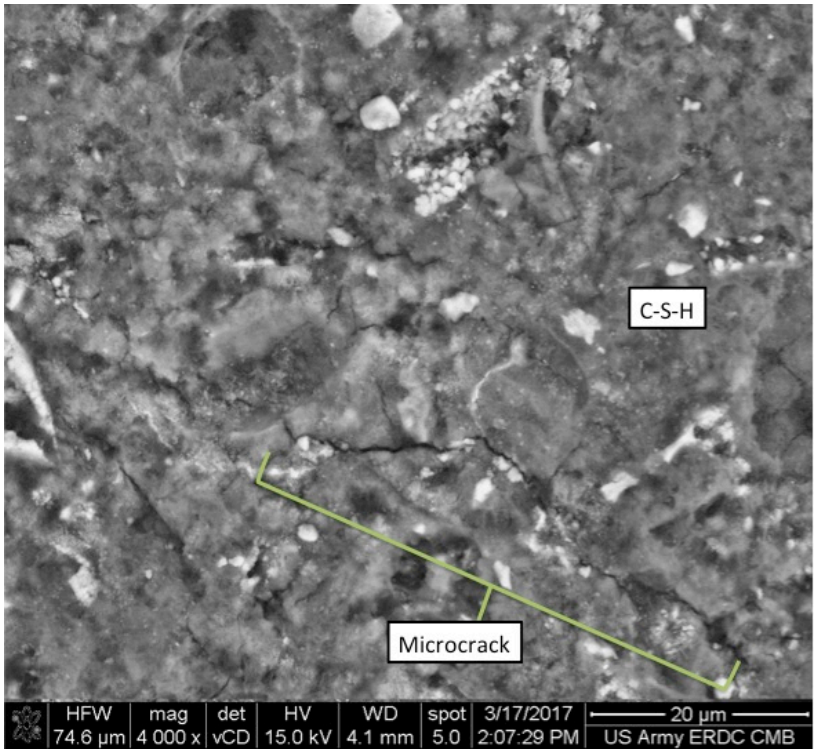

A 200x magnification montage image of the concrete microstructure for 170051-3 is shown in Figure 19 with phases indicated. Clays are primarily seen at the particle-paste boundary. They can be seen creating pathways between aggregate particles. High magnification images (Figure 20, 21) feature unhydrated cement particles, capillary pores, and some microcracking. The presence of secondary cementitious materials was not observed. Capillary pore space was qualitatively determined to suggest a water cement ratio of at least 0.55.

Figure 19. 200x magnification montage of microstructure for 170051-3 illustrating clay particles coating fine aggregate.

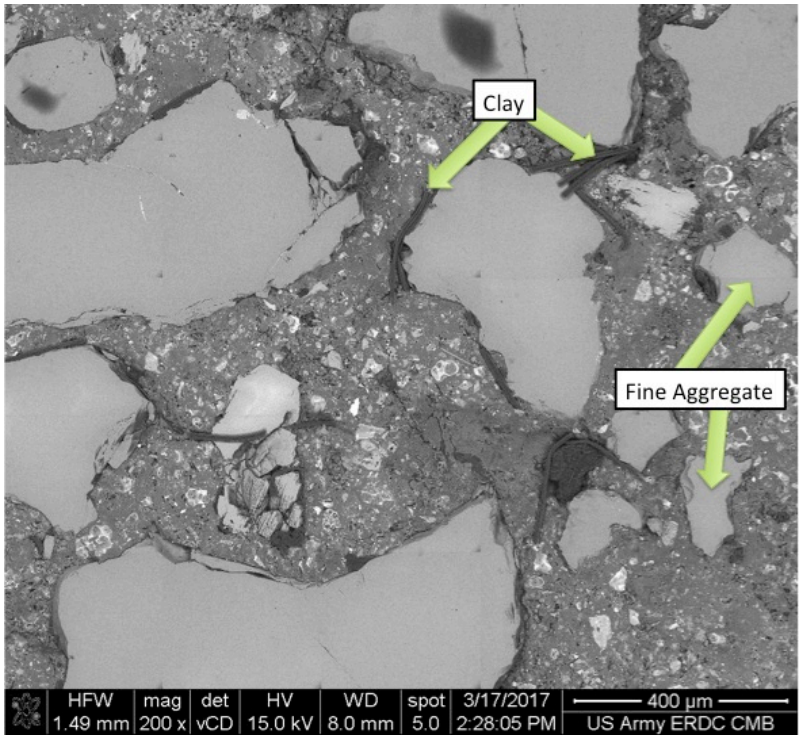

Figure 20. 1000x magnification image of concrete microstructure for 170051-3 illustrating clay coating on fine aggregate, high capillary porosity, high volume of unhydrated cement, and microcracking.

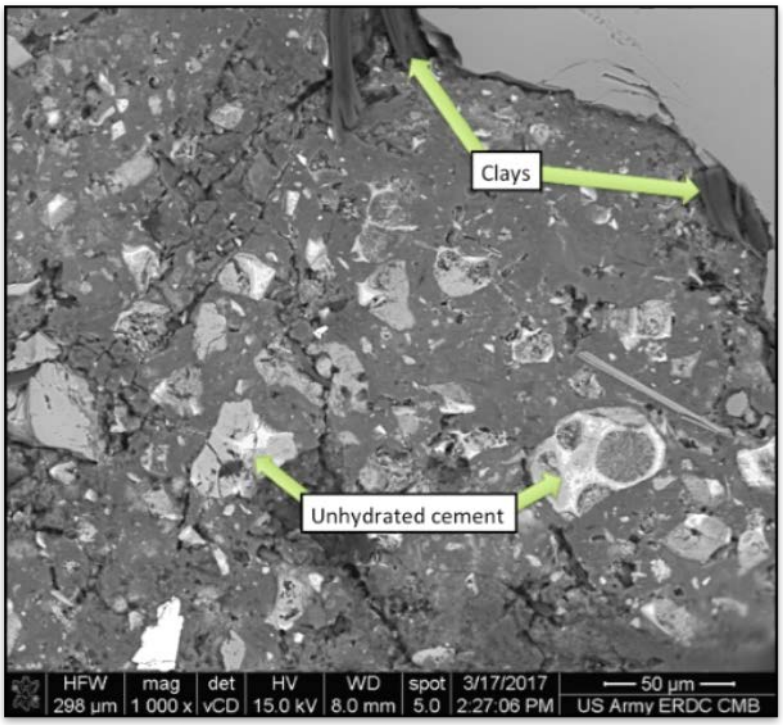

Figure 21. 2000x magnification image of concrete microstructure for 170051-3 illustrating capillary pores and microcracks, some of which have been infilled.

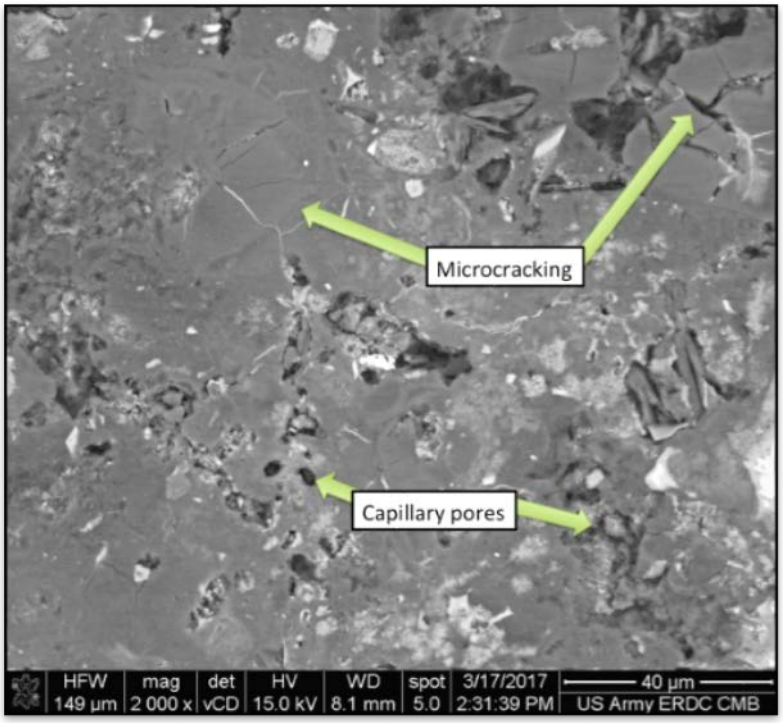

A 200x magnification montage image of the concrete microstructure for 170051-4 is shown in Figure 22 with phases indicated. Clays are primarily seen at the fine aggregate-paste boundary. High magnification images (Figure 23, 24) feature unhydrated cement particles, capillary pores, and some microcracking. The capillary pores can be seen creating large networks of void space. The presence of secondary cementitious materials was not observed. Capillary pore space suggests a water cement ratio of at least 0.55.

Figure 22. Low magnification montage of concrete microstructure for 170051-4.

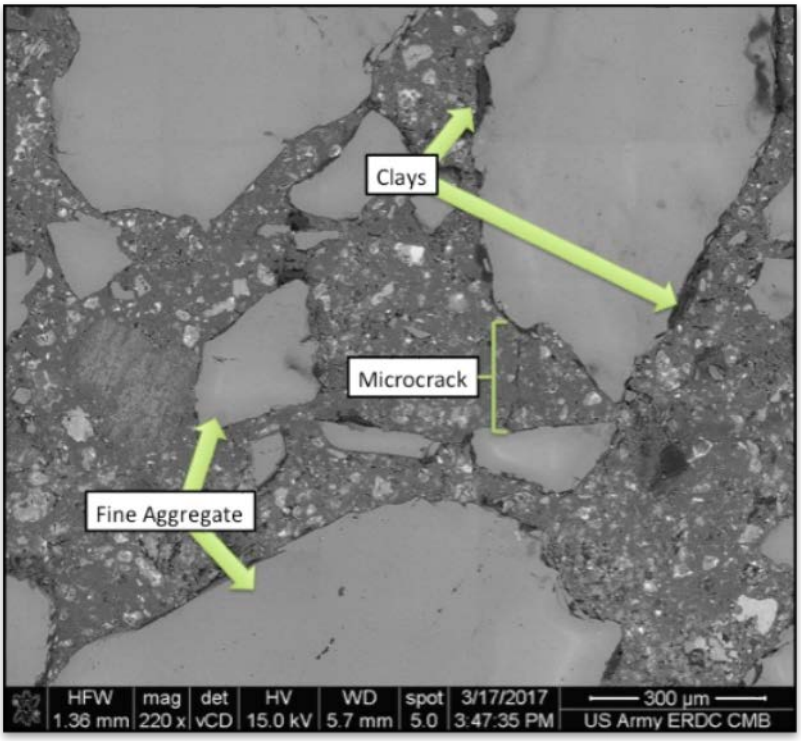

Figure 23. High magnification image of concrete microstructure for 170051-4.

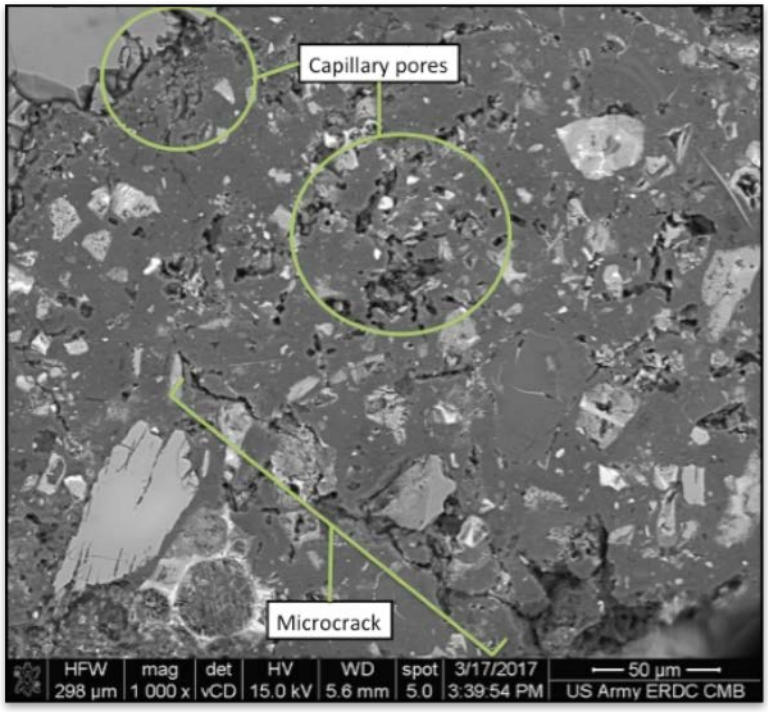

Figure 24. High magnification image of concrete microstructure for 170051-4. Large unhydrated cement grains also surrounded by microcracked hydrates as shown in circled area.

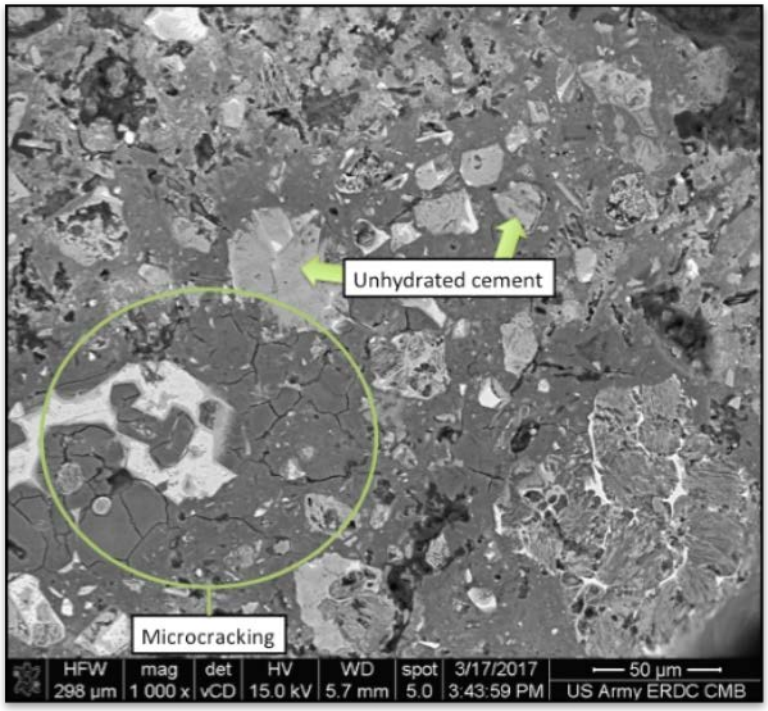

3.7 X-ray Diffraction Analysis

Diffraction patterns were gathered on the cement fraction of 170051-1-4. Calculated weight percentages of the cement minerals are shown in Table 2-5. The weight % composition for all phases identified is shown along with phases associated solely with the cementitious fraction (hydrated and anhydrous / unhydrated) which was then normalized to 100% total mass. The calculation focused on the solely cementitious fraction was to remove the inclusion of minerals associated with aggregates that were integrated into powders during specimen preparation and to aid in a comparison between the cementitious fraction in each core. Diffraction patterns and whole pattern fit analysis are shown in Figures 25 through 28. Each powder sample analyzed from cores 170051-1-4 included anticipated phases associated with unhydrated cement, the products of cement hydration, and minerals contributed by aggregates. Phases associated with unhydrated cement including alite, belite, and brownmillerite were observed in each sample and correlate with unhydrated cement grains that were also observed in SEM micrographs. Hydration products including phases associated with poorly-ordered calcium-silicate-hydrate, ettringite, and in the case of north wall cores portlandite was observed. High gypsum contents of up to 15 wt. % of the cementitious fraction were observed in south wall cores while gypsum contents were lower and portlandite contents were higher (up to 10 wt. %) in the north wall cores. The high gypsum content in south wall cores did not appear to be resulting in any observable deterioration based on microscopic observations. The poorly ordered calcium-silicate-hydrate phase was analyzed as a combination of C-S-H (tobermorite structure), hibschite (an aluminum doped polymorph of C-S-H), and amorphous material. The summation of these phases totaled approximately 50-60 wt. % of the cementitious fraction in each of the samples analyzed which is typical of hydrated portland cement paste. Minerals identified as being associated with the aggregate fraction and clay impurities included quartz, illite, albite, kaolinite, and microcline.

Table 2. Calculated weight percentages of materials identified through X-ray diffraction for 170051-1.

Mineral Name	Chemical Composition	Total Sample	Cementitious
		Wt. %	Wt. %
Quartz	SiO_2	28.4	-
C-S-H	$Ca_{2.5}Si_3O_9H$	8.4	20.6
Illite-2M2 (NR)	$(K,H_3O)Al_2(Si_3Al)O_{10}(OH)_2{\cdot}xH_2O$	10.7	-
Hibschite*	$Ca_3Al_2(SiO_4)_{1.25}(OH)_7$	10.2	23.5
Gypsum	$CaSO_4(H_2O)_2$	6.6	14.9
Albite	$(AlSi_3)NaO_8$	4.6	-
Ettringite	$Ca_3AlS_{1.5}O_{24.5}H_{31}$	1.3	3.4
Periclase	$(Mg_{0.6}Fe_{0.4})O$	0.3	1.0
Larnite	Ca_2SiO_4	6.3	13.5
Alite	Ca_3SiO_5	1.9	3.3
Brownmillerite	$Ca_2(Fe_{1.014}Al_{0.986})O_5$	0.2	0.6
Kaolinite 1A	$Al_2(Si_2O_5)(OH)_4$	1.6	-
Anhydrite	$Ca(SO_4)$	0.1	0.2
Microcline	$(K_{0.95}Na_{0.05})AlSi_3O_8$	10.9	-
Amorphous*	-	8.4	19.1

* Poorly ordered calcium silicate gel binding phase analyzed with multiple possible phases and amorphous material.

Table 3. Calculated weight percentages of materials identified through X-ray diffraction for 170051-2.

Mineral Name	Chemical Composition	Total Sample	Cementitious
		Wt. %	Wt. %
Quartz	SiO_2	22.2	-
Illite-2M2 (NR)	$(K,H_3O)Al_2(Si_3Al)O_{10}(OH)_2{\cdot}xH_2O$	6.1	12.5
Ettringite	$Ca_3AlS_{1.5}O_{24.5}H_{31}$	2.1	4.1
Hibschite*	$Ca_3Al_2(SiO_4)_{1.25}(OH)_7$	22.3	37.4
Gypsum	$CaSO_4(H_2O)_2$	7.6	14.3
C-S-H*	$Ca_{2.5}Si_3O_9H$	6.5	12.5
Larnite	Ca_2SiO_4	4.7	8.5
Microcline	$(K_{0.95}Na_{0.05})AlSi_3O_8$	9.9	-
Albite	$(AlSi_3)NaO_8$	6.0	1.2
Periclase	$(Mg_{0.6}Fe_{0.4})O$	0.5	-
Amorphous*	-	12.1	22.0

* Poorly ordered calcium silicate gel binding phase analyzed with multiple possible phases and amorphous material.

Table 4. Calculated weight percentages of materials identified through X-ray diffraction for 170051-3.

Mineral Name	Chemical Composition	Total Sample	Cementitious
		Wt. %	Wt. %
Quartz	SiO_2	19.5	-
Ettringite	$Ca_3AlS_{1.5}O_{24.5}H_{31}$	1.2	2.6
Monosulfate	$(Ca_2Al(OH)_6)(S_{0.5}O_2(OH_2)_3)$	13.0	25.2
Hibschite*	$Ca_3Al_2(SiO_4)_{1.25}(OH)_7$	23.2	44.5
Portlandite	$Ca(OH)_2$	3.3	6.3
Larnite	Ca_2SiO_4	1.3	4.8
Alite	Ca_3SiO_5	5.3	2.4
Gypsum	$CaSO_4(H_2O)_2$	4.3	7.7
Brownmillerite	$Ca_2(Fe_{1.014}Al_{0.986})O_5$	2.3	3.2
Albite	$(AlSi_3)NaO_8$	10.2	-
Microcline	$(K_{0.95}Na_{0.05})AlSi_3O_8$	14.8	-
Amorphous*	-	1.6	3.4

* Poorly ordered calcium silicate gel binding phase analyzed with multiple possible phases and amorphous material.

Table 5. Calculated weight percentages of materials identified through X-ray diffraction for 170051-4.

Mineral Name	Chemical Composition	Total Sample	Cementitious
		Wt. %	Wt. %
Quartz	SiO_2	19.1	-
Microcline	$(K_{0.95}Na_{0.05})AlSi_3O_8$	21	-
Ettringite	$Ca_3AlS_{1.5}O_{24.5}H_{31}$	1.9	3.6
Monosulfate	$(Ca_2Al(OH)_6)(S_{0.5}O_2(OH_2)_3)$	6.1	11
Albite	$(AlSi_3)NaO_8$	7.0	-
Hibschite*	$Ca_3Al_2(SiO_4)_{1.25}(OH)_7$	18.6	33
Portlandite	$Ca(OH)_2$	6.1	10.8
Larnite	Ca_2SiO_4	4.2	10.1
Brownmillerite	$Ca_2(Fe_{1.014}Al_{0.986})O_5$	1.9	1.9
Alite	Ca_3SiO_5	1.2	-
Mayenite	$(CaO)_{12}(Al_2O_3)_7$	0.3	0.6
C-S-H*	$Ca_{2.5}Si_3O_9H$	8.7	21.8
Amorphous*	-	3.9	7.2

* Poorly ordered calcium silicate gel binding phase analyzed with multiple possible phases and amorphous material.

Figure 25. Diffraction pattern for 170051-1 with phase identifications, whole pattern fit and calculated weight percentages.

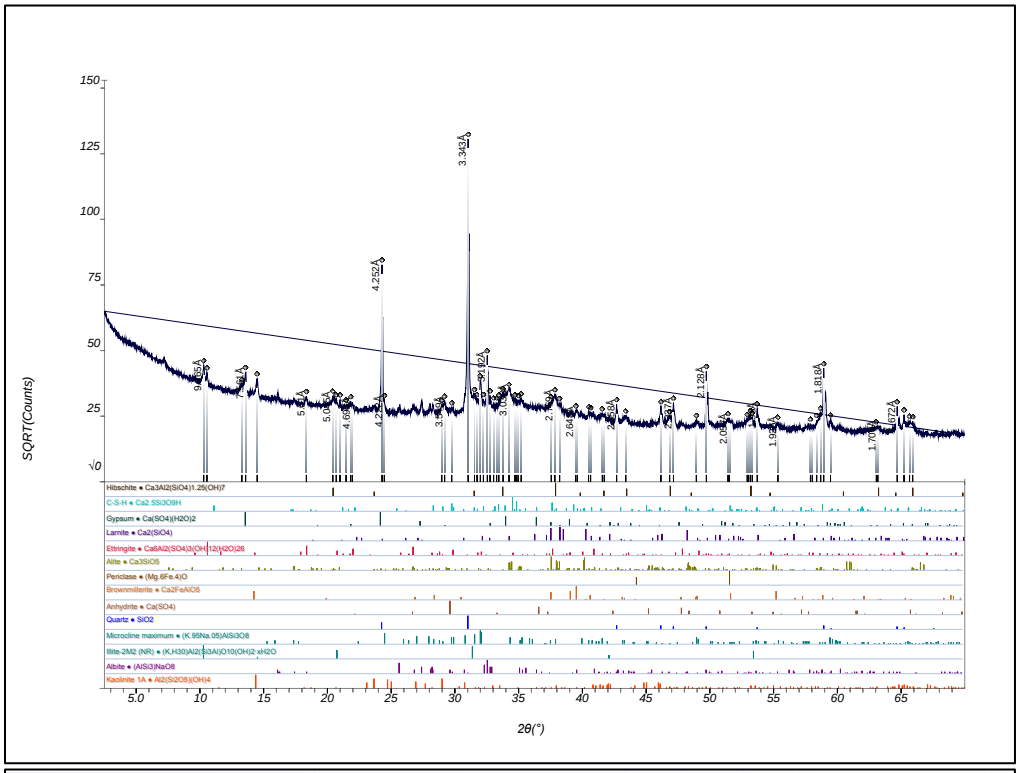

Phase ID (14)	Chemical Formula	NA	NR	NP	Wt% (esd)	RIR
Quartz	SiO2	---	12	9	28.4 (0.6)	3.04
Tobermorite	Ca2.5Si3O9H	15	174	4	8.4 (0.8)	0.51
Illite-2M2 (NR)	(K,H30)Al2(Si3Al)O10(OH)2·xH2O	---	6	*9	10.7 (1.2)	0.40
Hibschite	Ca3Al2(SiO4)1.25(OH)7	---	17	5	10.2 (0.5)	1.06
Gypsum	Ca(SO4)(H2O)2	---	54	4	6.6 (0.3)	1.91
Albite	(AlSi3)NaO8	17	155	11	4.6 (0.2)	1.08
Ettringite	Ca6Al2(SO4)3(OH)12(H2O)26	26	425	4	1.3 (0.2)	1.59
Periclase	(Mg.6Fe.4)O	3	2	4	0.3 (0.1)	3.61
Larnite	Ca2(SiO4)	7	93	4	6.3 (0.7)	0.69
Alite	Ca3SiO5	83	613	4	1.9 (0.4)	0.77
Brownmillerite	Ca2FeAlO5	---	35	3	0.2 (0.0)	2.24
Kaolinite 1A	Al2(Si2O5)(OH)4	---	114	7	1.6 (0.1)	1.08
Anhydrite | β-Ca (S O4)	Ca(SO4)	4	28	3	0.1 (0.0)	1.92
Microcline maximum	(K.95Na.05)AlSi3O8	---	113	4	10.9 (0.4)	0.58
Amorphous + Others	SiO2				8.4 (0.6)	2.60

XRF(Wt%): Fe2O3=0.3%, CaO=15.9%, K2O=2.4%, SO3=3.4%, SiO2=61.6%, Al2O3=10.2%, MgO=0.2%, Na2O=0.6%

Refinement Converged (R/E=2.02), ♣ Round=4, Iter=4, P=59, R=6.6% (E=3.27%, EPS=0.5)

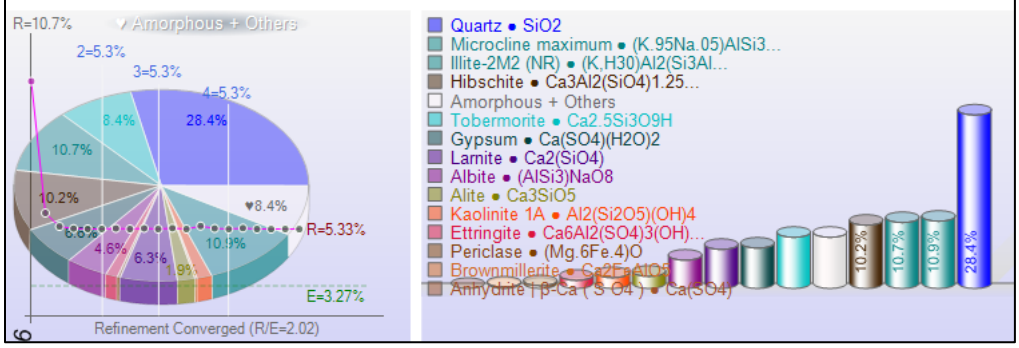

Figure 26. Diffraction pattern for 170051-2 with phase identifications, whole pattern fit and calculated weight percentages.

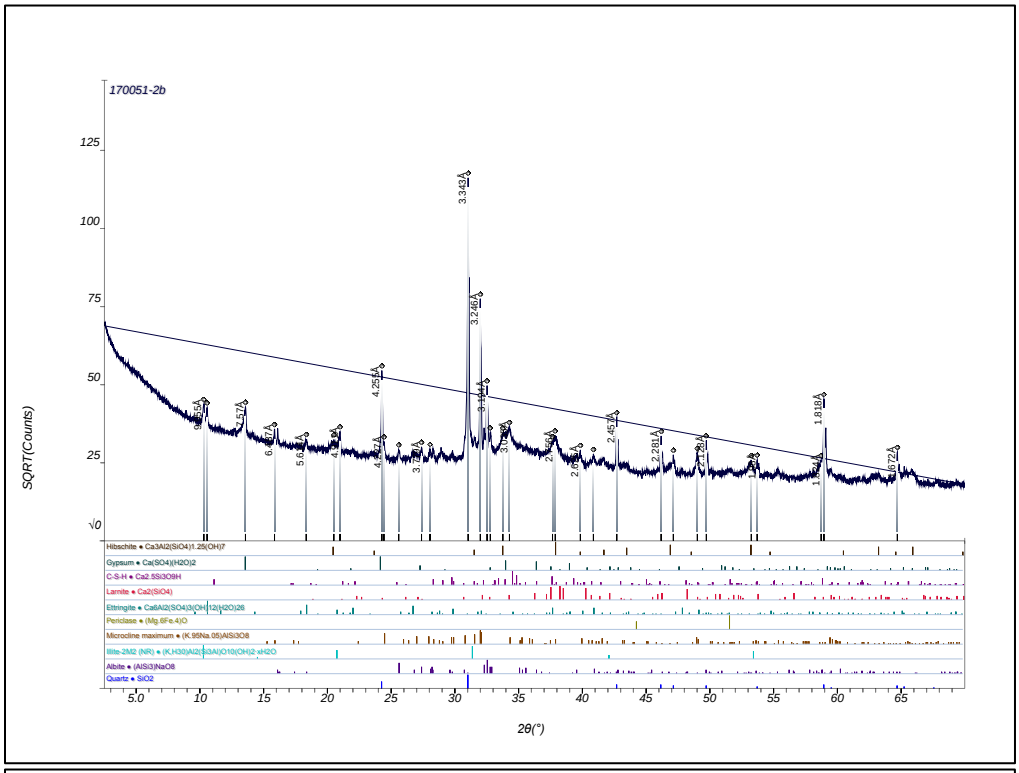

Phase ID (10)	Chemical Formula	PDF-#	NP	Wt% (esd)	RIR
Quartz	SiO2	01-075-0443	9	22.2 (0.5)	3.04
Illite-2M2 (NR)	(K,H30)Al2(Si3Al)O10(OH)2·xH2O	00-058-2015	*9	6.1 (1.3)	0.40
Ettringite	Ca6Al2(SO4)3(OH)12(H2O)26	04-011-5267	4	2.1 (0.2)	1.59
Hibschite	Ca3Al2(SiO4)1.25(OH)7	00-045-1447	5	22.3 (0.9)	1.06
Gypsum	Ca(SO4)(H2O)2	01-070-0982	4	7.6 (0.3)	1.91
C-S-H	Ca2.5Si3O9H	98-000-8489	4	6.5 (0.7)	0.51
Larnite	Ca2(SiO4)	04-008-1786	4	4.7 (0.6)	0.69
Microcline maximum	(K.95Na.05)AlSi3O8	01-084-1455	13	9.9 (0.2)	0.58
Albite	(AlSi3)NaO8	98-000-3287	11	6.0 (0.3)	1.08
Periclase	(Mg.6Fe.4)O	98-000-9483	4	0.5 (0.1)	3.61
Amorphous + Others	SiO2			12.1 (0.7)	2.60

XRF(Wt%): Fe2O3=0.3%, CaO=18.1%, K2O=1.9%, SO3=3.9%, SiO2=56.8%, Al2O3=11.0%, MgO=0.2%, Na2O=0.8%

Refinement Halted (R/E=1.97), ♣ Round=4, Iter=6, P=55, R=6.38% (E=3.24%, EPS=0.5)

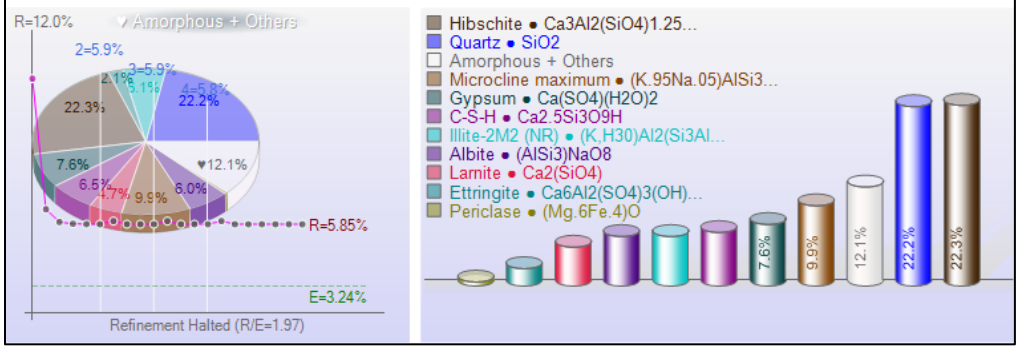

Figure 27 Diffraction pattern for 170051-3 with phase identifications, whole pattern fit and calculated weight percentages.

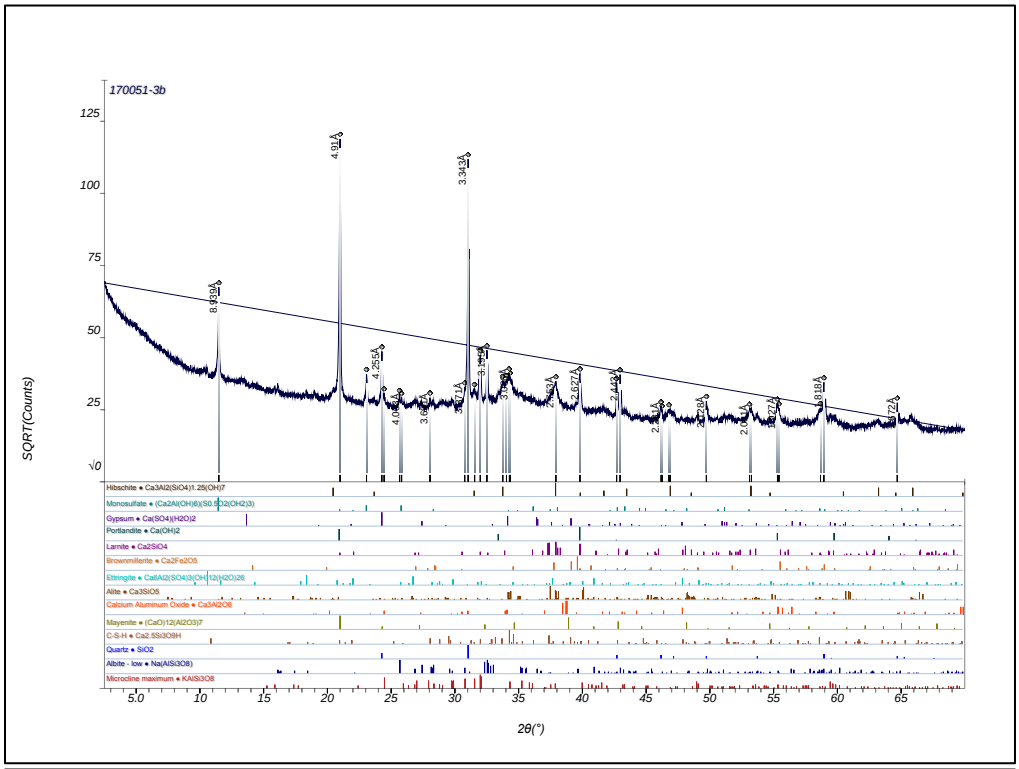

Phase ID (14)	Chemical Formula	PDF-#	NP	Wt% (esd)	RIR
Quartz	SiO2	98-000-0369	9	19.5 (0.5)	4.30
Ettringite	Ca6Al2(SO4)3(OH)12(H2O)26	04-011-5267	4	1.2 (0.3)	1.59
Monosulfate	(Ca2Al(OH)6)(S0.5O2(OH2)3)	01-083-1289	9	13.0 (0.3)	2.97
Hibschite	Ca3Al2(SiO4)1.25(OH)7	00-045-1447	5	23.2 (0.9)	1.06
Portlandite	Ca(OH)2	00-044-1481	4	3.3 (0.2)	2.90
Larnite	Ca2SiO4	98-001-4886	4	1.3 (0.5)	0.78
Alite	Ca3SiO5	98-001-4885	4	5.3 (1.0)	0.77
Gypsum	Ca(SO4)(H2O)2	01-072-0596	4	4.3 (0.2)	1.90
Mayenite	(CaO)12(Al2O3)7	01-070-2144	8	0.0 (0.0)	2.13
Brownmillerite	Ca2Fe2O5	98-001-0950	4	2.3 (0.5)	2.12
Calcium Aluminum Oxide	Ca3Al2O6	00-032-0148	*56	0.0 (0.0)	2.05
Tobermorite	Ca2.5Si3O9H	98-000-8489	10	0.0 (0.0)	0.51
Albite - low	Na(AlSi3O8)	98-000-0041	11	10.2 (0.4)	0.66
Microcline maximum	KAlSi3O8	01-076-0918	11	14.8 (0.4)	0.60
Amorphous + Others	SiO2			1.6 (0.8)	2.60

XRF(Wt%): Fe2O3=1.4%, CaO=24.2%, K2O=2.5%, SO3=3.9%, SiO2=43.8%, Al2O3=12.7%, Na2O=1.2%

Refinement Halted (R/E=1.53), ♣ Round=4, Iter=6, P=94, R=4.9% (E=3.20%, EPS=0.5)

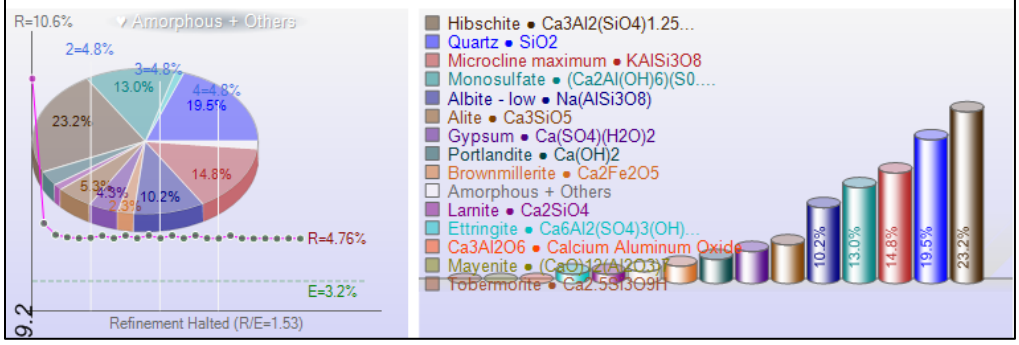

Figure 28. Diffraction pattern for 170051-4 with phase identifications, whole pattern fit and calculated weight percentages.

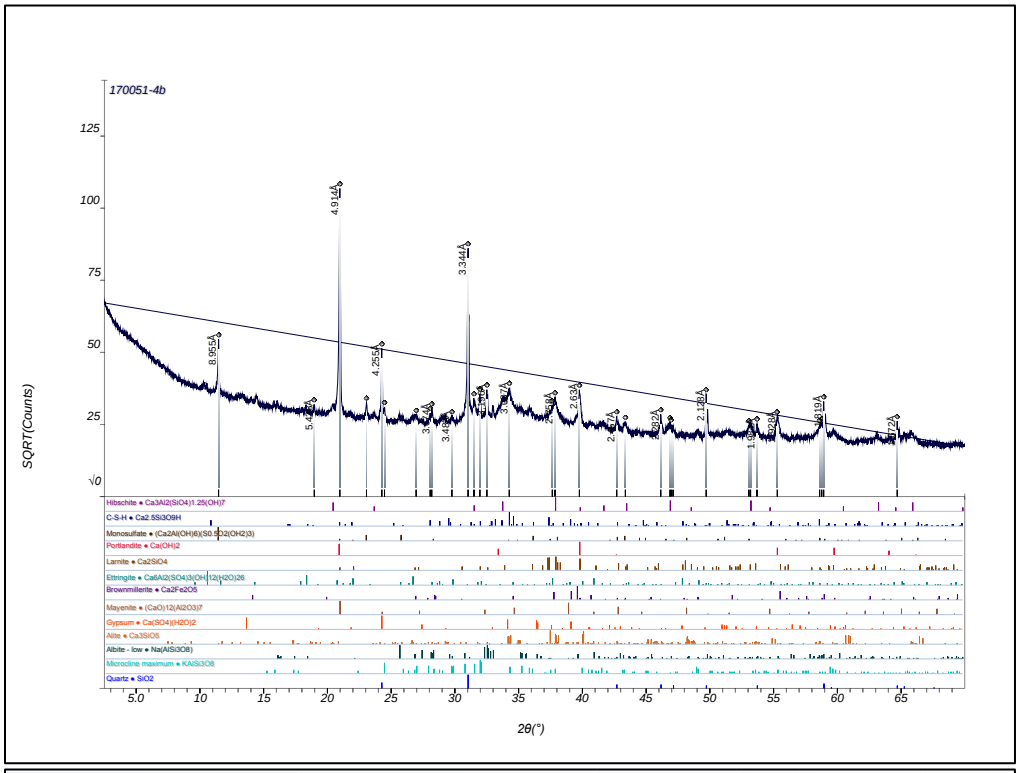

Phase ID (13)	Chemical Formula	PDF-#	NP	Wt% (esd)	RIR
Quartz	SiO2	98-000-0369	9	19.1 (0.4)	4.30
Microcline maximum	KAlSi3O8	01-076-0918	4	21.0 (1.0)	0.60
Ettringite	Ca6Al2(SO4)3(OH)12(H2O)26	04-011-5267	4	1.9 (0.5)	1.59
Monosulfate	(Ca2Al(OH)6)(S0.5O2(OH2)3)	01-083-1289	7	6.1 (0.1)	2.97
Albite - low	Na(AlSi3O8)	98-000-0041	4	7.0 (0.4)	0.66
Hibschite	Ca3Al2(SiO4)1.25(OH)7	00-045-1447	5	18.6 (0.8)	1.06
Portlandite	Ca(OH)2	00-044-1481	6	6.1 (0.3)	2.90
Larnite	Ca2SiO4	98-001-4886	4	4.2 (0.8)	0.78
Brownmillerite	Ca2Fe2O5	98-001-0950	4	1.9 (0.5)	2.12
Alite	Ca3SiO5	98-001-4885	4	1.2 (0.4)	0.77
Gypsum	Ca(SO4)(H2O)2	01-072-0596	11	0.0 (0.0)	1.90
Mayenite	(CaO)12(Al2O3)7	01-070-2144	8	0.3 (0.0)	2.13
C-S-H	Ca2.5Si3O9H	98-000-8489	11	8.7 (1.2)	0.51
Amorphous + Others	SiO2			3.9 (0.6)	2.60

XRF(Wt%): Fe2O3=1.1%, CaO=23.3%, K2O=3.5%, SO3=1.2%, SiO2=51.4%, Al2O3=11.2%, Na2O=0.8%

Refinement Halted (R/E=1.59), ♣ Round=4, Iter=6, P=61, R=5.22% (E=3.28%, EPS=0.5)

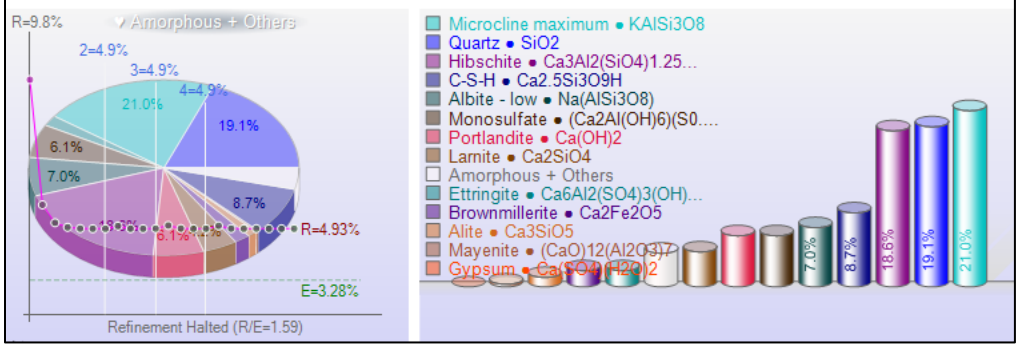

3.8 Chemical Spray Indicator Testing

The application of sodium cobaltinitrite and rhodamine B to the surface of the concrete are indicator methods to identify the presence of ASR. Due to the absence of staining by both sprays, it was concluded that ASR processes have not taken place (Figure 29a and b, Figure 30a and b).

Phenolphthalein, a pH indicator, was applied to core 170051-1 that was observed to have two distinct regions of paste according to color (Figure 29c) and the only exposed exterior surface in the as-received cores. The test indicated that the moderate orange pink area has a pH of less than or equal to 10, suggesting carbonation of the concrete at a higher rate than is expected. This carbonation seems linked with the sheet pile panel it was in contact with. It was also applied to 170051-3 (Figure 30c) and no carbonation was observed.

Figure 29. Various chemical sprays applied to core sample 170051-1 (a) sodium cobaltinitrite showing no reaction (b) rhodamine B highlighting carbonated cement with a bright pink stain (c) Phenolphthalein indicating the top portion of the sample having a pH of less than 8.6

(a) Sodium Cobaltinitrite

(b) Rhodamine B

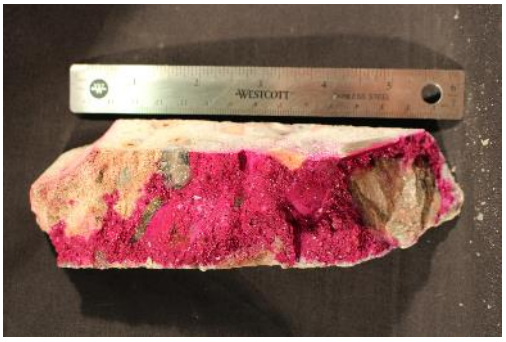

(c) Phenolphthalein

Figure 30. Various chemical sprays applied to core sample 170051-3 (a) sodium cobaltinitrite showing no reaction (b) rhodamine B showing little reaction (c) Phenolphthalein indicating no carbonation

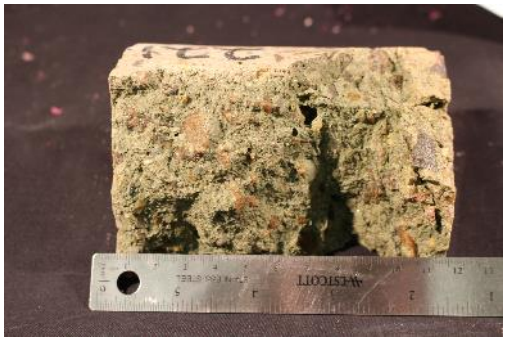

(a) Sodium Cobaltinitrite

(b) Rhodamine B

(c) Phenolphthalein

3.9 Air Void Analysis ASTM-C457 / Phase Fraction Analysis

The minimum length of traverse and minimum number of points for the point count method were determined based on the maximum size of aggregate found in each sample. For this study, the nominal aggregate size used was 1.5 in. Sample 170051-1 had an air content of 3.2% and paste volume fraction was 34.7%, void frequency (n) was 1.2, paste-to-air ratio (p/A) was 10.8, and the spacing factor (L) was 0.017 in. (1.1 mm). Sample 170051-2 had an air content of 3.4% and paste volume fraction was 25.4%, void frequency (n) was 1.0, paste-to-air ratio (p/A) was 7.4, and the spacing factor (L) was 0.015 in. (1.1 mm). Sample 170051-3 had an air content of 5.0% and paste volume fraction was 25.0%, void frequency (n) was 2.1, paste-to-air ratio (p/A) was 5.0, and the spacing factor (L) was 0.007 in. (1.1 mm). Sample 170051-4 had an air content of 7.1% and paste volume fraction was 27.8%, void frequency (n) was 1.5, paste-to-air ratio (p/A) was 3.9, and the spacing factor (L) was 0.0107 in. (1.1 mm). Sample 170051-5

had an air content of 1.3% and paste volume fraction was 37.3%, void frequency (n) was 0.8, paste-to-air ratio (p/A) was 28.2, and the spacing factor (L) was 0.0258in. (1.1 mm). (See Appendix B for all calculations) Mixture proportions for each sample were calculated based on data gathered from ASTM C-457 and are listed in Table 3. Overall the results indicate a fairly similar mixture proportion as used in the north and south walls with increased air content in north wall samples. Limitations on the analysis area of sample 170051-5 due to the as-received geometry make conclusions from its analysis unclear.

Table 6. Percentage of concrete constituents based on ASTM C-457 analysis.

Concrete Phase Fraction		170051-1	170051-2	170051-3	170051-4	170051-5
Air	A%	3.21	3.42	5.02	7.1	1.32
Paste	P%	34.74	25.38	25.03	27.83	37.29
Fine Aggregate	fa%	25.97	20.54	20.36	22.4	29.69
Coarse Aggregate	ca%	35.55	50.19	49.39	42.66	31.70

4 Summary and Conclusions

This study examined four concrete cores from the north and south walls of the H-Canyon Exhaust Tunnel (HCAEX). The five cores, which were logged in as CMB No. 170051-1 to 05 were subjected to an in-depth analysis consisting of visual and petrographic examination, chemical spray indicators, electron microscopy, x-ray diffraction, and hardened concrete air void analysis. The results of the study were:

- Macroscopic cores were not observed in the provided cores. Proportions of concrete phases were in the standard range.

- Core 170051-1 had two distinct regions of paste according to color. The moderate orange pink that extended ~1 ½ inches. This area reacted with phenolphthalein suggesting a distinct carbonated zone where contact was made with the exterior surface.

- Cores from the south wall has a grey (N7) paste, while the paste from the north wall is pale yellowish brown (10YR 6/2). Energy-dispersive electron microscopy suggests a slight variation in chemistry may be at fault along with an increased abundance of clay in the north wall.

- No evidence of alkali-silica reaction was observed such as internal microcracks filled with gel. This was true in all core samples analyzed.

- High magnification electron microscopy revealed anticipated phases. A large proportion of unhydrated cement particles were observed dispersed in hydrated cement paste, suggesting a high water/cement ratio. No supplementary cementitious materials were observed such as residual textures from fly ash or slag. This is supported by a lack of non-reactive refractory phases such as mullite or iron oxides in paste XRD patterns which are commonly associated with supplementary cementitious materials.

- The capillary porosity is extensive, especially in north wall samples. As such, the cement/water ratio is qualitatively determined to be at least 0.50, likely higher in the north wall. This is corroborated by a

determined non-evaporable water loss (mass loss difference between 105-1000 °C) average of the cement fraction from each core sample, which was measured on paste samples. The south wall samples had an average water loss of 18.5% by mass while the north wall samples had an average of 21.4% by mass.

- The presence of clay is seen in the concrete microstructure via electron microscopy and validated by x-ray diffraction results. Clay particles are primarily found at the paste-coarse and fine aggregate boundary but are also isolated in the cement. The origin of these clays is unclear but is likely due to poor aggregate washing. The abundance of clay minerals likely contributed to the loss in strength as the particles interfere with the aggregate/paste interface, weakening their adhesion.

- X-ray diffraction results indicated anticipated phases present in the cement paste including residual unhydrated portland cement phases alite, belite, and brownmillerite along with the results of cement hydration such as ettringite, portlandite, and poorly-ordered calcium-silicate-hydrate (tobermorite, hibschite, and amorphous material). Contributions from the aggregate were also observed in XRD results but were not considered for comparisons between paste compositions in the north and south wall specimens.

- Small microcracks (~10 μm) were seen throughout all samples. Some of them appear to be infilled, probably by mineral phases. These were likely formed due to shrinkage.

- Results of air void analysis of the 2 samples from the south wall yielded similar results, while samples from the north wall had variations in percent air content. Calculated mixture proportions for all the samples were roughly the same.

Overall, the concrete did not appear to have been subjected to deleterious chemical alteration or reactions such as sulfate attack, ASR, or carbonation. As such, the concrete is not expected to lose strength in the future due to normal aging. Cracking of the concrete and aggregate was largely absent. Electron microscopy indicates the presence of abundant clay particles (kaolinite) within the concrete, especially in the north wall. These clay

particles are observed coating the aggregate, which can cause a loss of adhesion between the aggregate and paste. This is the likely culprit for the observed low strength in the north wall along with the increased abundance of high capillary porosity and high air content observed in north wall samples.

5 References

ASTM C457/C457M-12 *Standard Test Method for Microscopical Determination of Parameters of the Air-Void System in Hardened Concrete,* ASTM International, West Conshohocken, PA, 2012, https://doi.org/10.1520/C0457_C0457M-12

ASTM C856 – 17 *Standard Practice for Petrographic Examination of Hardened Concrete,* ASTM International, West Conshohocken, PA

ASTM C1365 – Standard Test Method for Determination of the Proportion of Phases in Portland Cement and Portland-Cement Clinker Using X-Ray Powder Diffraction Analysis, ASTM International, West Conshohocken, PA

ASTM C1723 – *Standard Guide for Examination of Hardened Concrete Using Scanning Electron Microscopy*, ASTM International, West Conshohocken, PA

Rivard, Patrice, Benoit Fournier, and Gerard Ballivy. 2002. The Damage Rating Index Method for ASR Affected Concrete – A Critical Review of Petrographic Features of Deterioration and Evaluation Criteria. Cement, Concrete, and Aggregates, vol. 24. pg.1-10.

St. John, Donald A., Alan W. Poole, and Ian Simms. 1998. Concrete Petrography, A Handbook of Investigative Techniques. John Wiley and Sins, Inc. 605 Third Avenue, New York, NY 10158

Contact Information

For any questions related to the results of this study please contact:

Cody M. Strack, G.I.T.
Research Geologist
Concrete and Materials Branch
Geotechnical and Structural Laboratory
U.S. Army Engineer Research and Development Center
Office: (601) 634-7442
Cody.strack@usace.army.mil

E. Rae Reed-Gore, G.I.T.
Research Geologist
Concrete and Materials Branch
Geotechnical and Structural Laboratory
U.S. Army Engineer Research and Development Center
Office: (601) 634-2235
Erin.R.Gore@usace.army.mil

Robert D. Moser, Ph.D.
Senior Research Civil Engineer
Engineering Systems and Materials Division – Research Group
Geotechnical and Structural Laboratory
U.S. Army Engineer Research and Development Center
Phone: (601) 634-3261
Robert.D.Moser@usace.army.mil

Appendix A: Core Log Sheet

Hole No.

DRILLING LOG	DIVISION	INSTALLATION	SHEET OF SHEETS
1. PROJECT DOE Savannah River Site 170051-2		10. SIZE AND TYPE OF BIT	
2. LOCATION (Coordinates or Station) 221H-PT3-S6D		11. DATUM FOR ELEVATION SHOWN (TBM or MSL)	
3. DRILLING AGENCY (1/23/14)		12. MANUFACTURER'S DESIGNATION OF DRILL	
4. HOLE NO. (As shown on drawing title and file number)		13. TOTAL NO. OF OVER-BURDEN SAMPLES TAKEN	DISTURBED / UNDISTURBED
5. NAME OF DRILLER		14. TOTAL NUMBER CORE BOXES	
6. DIRECTION OF HOLE ☐ VERTICAL ☐ INCLINED _____ DEG. FROM VERT.		15. ELEVATION GROUND WATER	
		16. DATE HOLE	STARTED / COMPLETED
7. THICKNESS OF OVERBURDEN		17. ELEVATION TOP OF HOLE	
8. DEPTH DRILLED INTO ROCK		18. TOTAL CORE RECOVERY FOR BORING	%
9. TOTAL DEPTH OF HOLE		19. SIGNATURE OF INSPECTOR	

ELEVATION a	DEPTH (ft) b	LEGEND c	CLASSIFICATION OF MATERIALS (Description) d	% CORE RECOVERY e	BOX OR SAMPLE NO. f	REMARKS (Drilling time, water loss, depth of weathering, etc., if significant) g
	1		↑ Air fract. w/in Ass "pink" rim porto	XRD	several fracture pt	3¾" 6" long 1½-2" QA granitic/gneiss
	2					
	3					
	4					
	5					
	6					
	7		↑ joint surface? ↑ variations in porosity			

ENG FORM 1836 MAR 71 PREVIOUS EDITIONS ARE OBSOLETE. PROJECT HOLE NO.

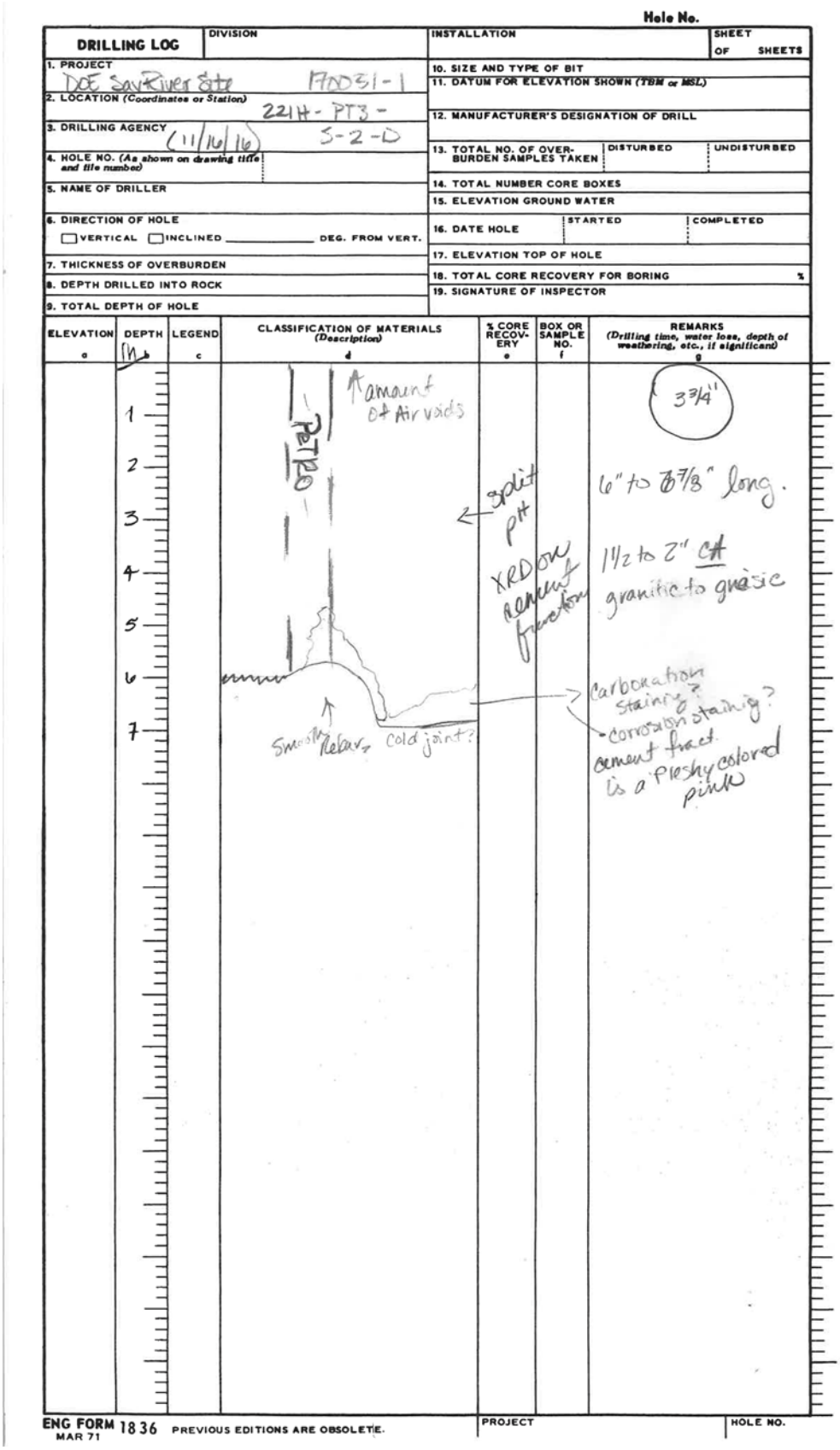

Hole No.

DRILLING LOG | DIVISION | INSTALLATION | SHEET OF SHEETS

1. PROJECT: DOE Savannah River Site — 17003I-1
2. LOCATION (Coordinates or Station): 221H - PT3 - S-2-D
3. DRILLING AGENCY: (11/16/16)
4. HOLE NO. (As shown on drawing title and file number)
5. NAME OF DRILLER
6. DIRECTION OF HOLE: ☐ VERTICAL ☐ INCLINED _____ DEG. FROM VERT.
7. THICKNESS OF OVERBURDEN
8. DEPTH DRILLED INTO ROCK
9. TOTAL DEPTH OF HOLE
10. SIZE AND TYPE OF BIT
11. DATUM FOR ELEVATION SHOWN (TBM or MSL)
12. MANUFACTURER'S DESIGNATION OF DRILL
13. TOTAL NO. OF OVER-BURDEN SAMPLES TAKEN | DISTURBED | UNDISTURBED
14. TOTAL NUMBER CORE BOXES
15. ELEVATION GROUND WATER
16. DATE HOLE | STARTED | COMPLETED
17. ELEVATION TOP OF HOLE
18. TOTAL CORE RECOVERY FOR BORING %
19. SIGNATURE OF INSPECTOR

ELEVATION a	DEPTH (ft)	LEGEND c	CLASSIFICATION OF MATERIALS (Description) d	% CORE RECOVERY e	BOX OR SAMPLE NO. f	REMARKS (Drilling time, water loss, depth of weathering, etc., if significant) g
	1–7		Amount of Air voids; PT2D; split pt; XRD on cement fraction; Smooth Rebar; Cold joint?			3 3/4"; 6" to 6 7/8" long.; 1 1/2 to 2" CA granitic to gneisic; carbonation staining? - corrosion staining? cement fract. is a fleshy colored pink

ENG FORM 1836 MAR 71 PREVIOUS EDITIONS ARE OBSOLETE. | PROJECT | HOLE NO.

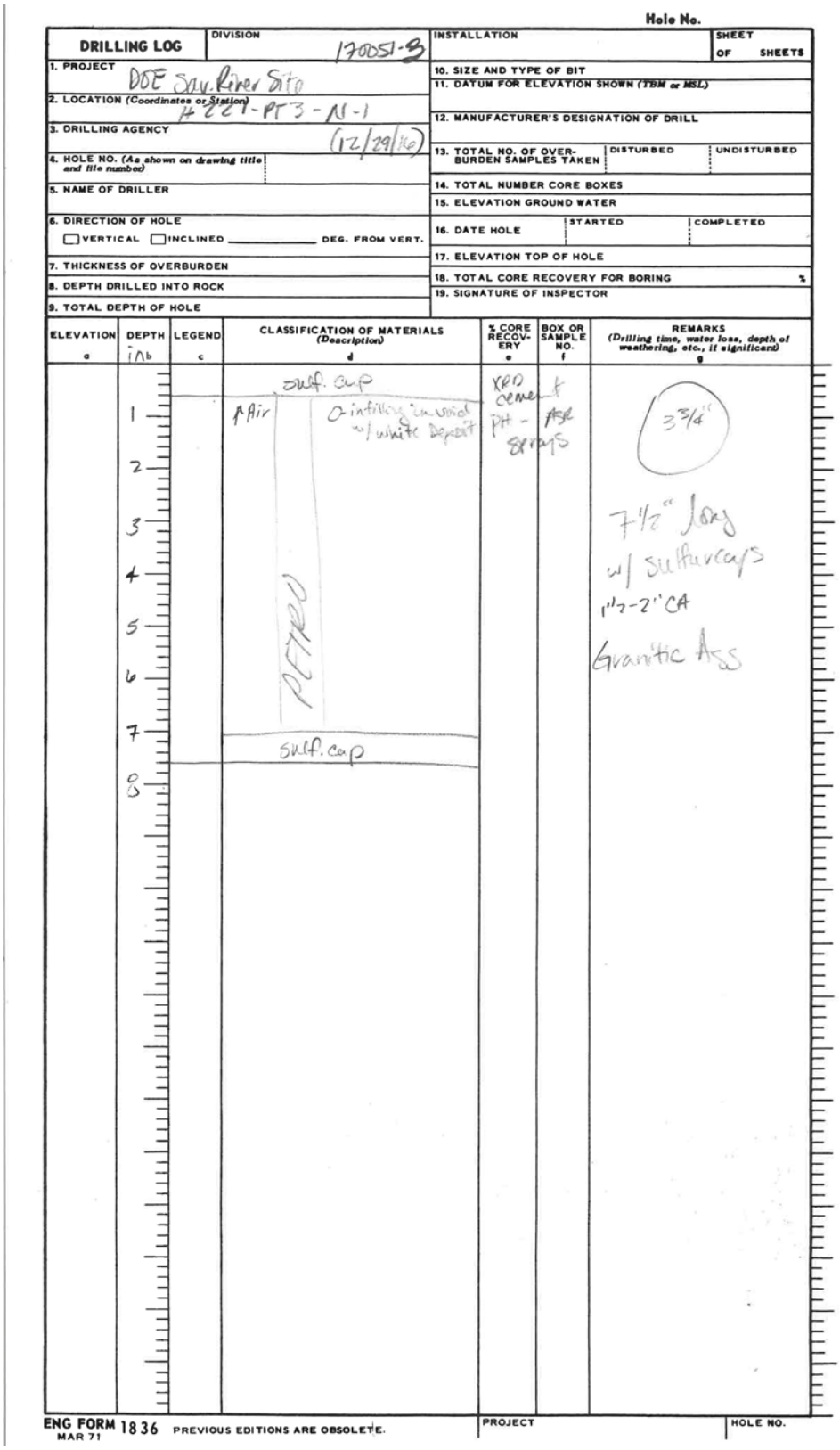

Hole No.

DRILLING LOG | DIVISION 17005-S | INSTALLATION | SHEET OF SHEETS

1. PROJECT: DOE Sav. River Site
2. LOCATION (Coordinates or Station): H-22-PT3-N-1
3. DRILLING AGENCY: (12/29/16)
4. HOLE NO. (As shown on drawing title and file number)
5. NAME OF DRILLER
6. DIRECTION OF HOLE: ☐ VERTICAL ☐ INCLINED _____ DEG. FROM VERT.
7. THICKNESS OF OVERBURDEN
8. DEPTH DRILLED INTO ROCK
9. TOTAL DEPTH OF HOLE
10. SIZE AND TYPE OF BIT
11. DATUM FOR ELEVATION SHOWN (TBM or MSL)
12. MANUFACTURER'S DESIGNATION OF DRILL
13. TOTAL NO. OF OVER-BURDEN SAMPLES TAKEN | DISTURBED | UNDISTURBED
14. TOTAL NUMBER CORE BOXES
15. ELEVATION GROUND WATER
16. DATE HOLE | STARTED | COMPLETED
17. ELEVATION TOP OF HOLE
18. TOTAL CORE RECOVERY FOR BORING %
19. SIGNATURE OF INSPECTOR

ELEVATION a	DEPTH in b	LEGEND c	CLASSIFICATION OF MATERIALS (Description) d	% CORE RECOVERY e	BOX OR SAMPLE NO. f	REMARKS (Drilling time, water loss, depth of weathering, etc., if significant) g
	0		surf. cap	XRD cores + pH - Aqe extracts		3 3/4"
	1		Air / 0-intrusive "in void w/ white deposit			7 1/2" long w/ sulfur caps 1 1/2-2" CA Granitic Ass
	2					
	3					
	4					
	5					
	6					
	7		surf. cap			
	8					

ENG FORM 1836 MAR 71 PREVIOUS EDITIONS ARE OBSOLETE. | PROJECT | HOLE NO.

Hole No.

DRILLING LOG	DIVISION	INSTALLATION	SHEET OF SHEETS

1. PROJECT: DOE Savannah River Site / 700S1-4
2. LOCATION (Coordinates or Station): 221-H-PTS-N-2-B
3. DRILLING AGENCY: (12/29/16)
4. HOLE NO. (As shown on drawing title and file number)
5. NAME OF DRILLER
6. DIRECTION OF HOLE: ☐ VERTICAL ☐ INCLINED _____ DEG. FROM VERT.
7. THICKNESS OF OVERBURDEN
8. DEPTH DRILLED INTO ROCK
9. TOTAL DEPTH OF HOLE
10. SIZE AND TYPE OF BIT
11. DATUM FOR ELEVATION SHOWN (TBM or MSL)
12. MANUFACTURER'S DESIGNATION OF DRILL
13. TOTAL NO. OF OVER-BURDEN SAMPLES TAKEN | DISTURBED | UNDISTURBED
14. TOTAL NUMBER CORE BOXES
15. ELEVATION GROUND WATER
16. DATE HOLE | STARTED | COMPLETED
17. ELEVATION TOP OF HOLE
18. TOTAL CORE RECOVERY FOR BORING %
19. SIGNATURE OF INSPECTOR

ELEVATION a	DEPTH b	LEGEND c	CLASSIFICATION OF MATERIALS (Description) d	% CORE RECOVERY e	BOX OR SAMPLE NO. f	REMARKS (Drilling time, water loss, depth of weathering, etc., if significant) g
	1		sulfur CAP			
	2		↑Air, some drilling	Petro	DH hose sprays	6"
	3				XRD cement	1 1/2" long w/ sulfur caps
	4					
	5					1 1/2" - 2" CA
	6					
	7					
	8					
	9					
	10					
	11		sulfur CAP			
	12					

ENG FORM 1836 MAR 71 PREVIOUS EDITIONS ARE OBSOLETE. PROJECT HOLE NO.

Appendix B: ASTM C-457 air void analysis calculated results

170051-1	Distance traversed E-W (in)	5.5	in
Calculations:	Number of Traverses	17	

Total number of air voids intersected	N	113				
Total number of Stops	St	2461		Entrained		Entrapped
Number of stops in air voids	Sa	79	Sa	55	Sa	24
Number of stops in paste	Sp	855				
E-W translation distance between stops	l	0.037993				

Total Traverse Length	Tt	93.5				
Air Content	A %	3.2				
Void Frequency	n	1.2				
Paste Content %	p	34.7				
Paste-Air ratio	p/A	10.8	Entrained	2.234864	Entrapped	0.975213
Average chord length	l in	0.027				
Specific Surface	α in2/in3	150.6				

Spacing Factor	L in	0.016551519	if P/A less than 4.342		
	4.342L=	0.071866696			
	4.342L=	0.089888871	4.342L=	0.089989	if P/A greater than 4.342
		0.019920944	L=	0.020725	
		3.94092827			

170051-2		Distance traversed E-W (in)	5.59	in					
Calculations:		Number of Traverses	17						
Total number of air voids intersected			N	92					
Total number of Stops			St	2313		Entrained		Entrapped	
Number of stops in air voids			Sa	79	Sa	31	Sa	48	
Number of stops in paste			Sp	587					
E-W translation distance between stops			l	0.041085					
Total Traverse Length		Tt	95.0						
Air Content		A %	3.4						
Void Frequency		n	1.0						
Paste Content %		p	25.4						
Paste-Air ratio		p/A	7.4		Entrained	1.340251	Entrapped	2.075227	
Average chord length		l in	0.035						
Specific Surface		α in2/in3	113.4						
Spacing Factor		L in	0.015093347	if P/A less than 4.342					
		4.342L=	0.065535313						
		4.342L=	0.077637575	4.342L=	0.077638	if P/A greater than 4.342			
			0.026459743	L=	0.017881				
			2.810126582						

170051-3	Distance traversed E-W (in)		6.29	in					
Calculations:	Number of Traverses		16						
Total number of air voids intersected			N	210					
Total number of Stops			St	2549		Entrained		Entrapped	
Number of stops in air voids			Sa	128	Sa	47	Sa	81	
Number of stops in paste			Sp	638					
E-W translation distance between stops			l	0.039482					
Total Traverse Length	Tt	100.6							
Air Content	A %	5.0							
Void Frequency	n	2.1							
Paste Content %	p	25.0							
Paste-Air ratio	p/A	5.0			Entrained	1.84386	Entrapped	3.177717	
Average chord length	l in	0.024							
Specific Surface	α in2/in3	166.2							
Spacing Factor	L in	0.00690641	if P/A less than 4.342						
	4.342L=	0.029987633							
	4.342L=	0.032356562	4.342L=	0.032357	if P/A greater than 4.342				
		0.018048983	L=	0.007452					
		1.994791667							

170051-4	Distance traversed E-W (in)		4.76	in					
Calculations:	Number of Traverses		31						
Total number of air voids intersected			N	221					
Total number of Stops			St	2576		Entrained		Entrapped	
Number of stops in air voids			Sa	183	Sa	53	Sa	130	
Number of stops in paste			Sp	717					
E-W translation distance between stops			l	0.057283					
Total Traverse Length	Tt	147.6							
Air Content	A %	7.1							
Void Frequency	n	1.5							
Paste Content %	p	27.8							
Paste-Air ratio	p/A	3.9			Entrained	2.057453	Entrapped	5.046584	
Average chord length	l in	0.047							
Specific Surface	α in2/in3	84.3							
Spacing Factor	L in	0.010700396	if P/A less than 4.342						
	4.342L=	0.04646112							
	4.342L=	0.046072324	4.342L=	0.046072	if P/A greater than 4.342				
		0.035574833	L=	0.010611					
		1.639344262							

170051-5	Distance traversed E-W (in)	3.9	in					
Calculations:	Number of Traverses	25						
Total number of air voids intersected		N	81					
Total number of Stops		St	2041		Entrained		Entrapped	
Number of stops in air voids		Sa	27	Sa	27	Sa	0	
Number of stops in paste		Sp	761					
E-W translation distance between stops		l	0.047771					
Total Traverse Length	Tt	97.5						
Air Content	A %	1.3						
Void Frequency	n	0.8						
Paste Content %	p	37.3						
Paste-Air ratio	p/A	28.2		Entrained	1.322881	Entrapped	0	
Average chord length	l in	0.016						
Specific Surface	α in2/in3	251.2						
Spacing Factor	L in	0.025841126	if P/A less than 4.342					
	4.342L=	0.11220217						
	4.342L=	0.150713612	4.342L=	0.150714	if P/A greater than 4.342			
		0.011942675	L=	0.034711				
		9.728395062						